DESIGN, FABRICATION, AND TEST OF THE RL10 DERIVATIVE II CHAMBER/PRIMARY NOZZLE

FINAL REPORT

Pratt & Whitney
Government Engine Business
P.O. Box 109600
West Palm Beach, Florida 33410-9600

(NASA-CR-179555) DESIGN, FREFICATION AND
N89-23519
TEST OF THE BI10 DEFIVATIVE 11
CHAMBER/FRIMARY ACZZLE Final Report, Nov.
1984 - Nov. 1986 (Pratt and Whitney
Liccraft) 136 p
Unclas

April 1989

Prepared for: Lewis Research Center Under Contract NAS3-24738



FOREWORD

This report presents the RL10-II chamber/primary nozzle design, fabrication, and test.

Design of the chamber/primary nozzle was begun in the summer of 1982 and fabrication of the first assembly was completed in 1984. Testing was accomplished in March 1986. Delay of the testing was due to test stand usage for the Shuttle/Centaur program.

The design, fabrication and test of the RL10-II chamber/primary nozzle was conducted under the direction of NASA/LeRC with Mr. James Burkhart as Program Manager and Mr. Richard DeWitt as Technical Monitor. The effort at Pratt & Whitney was performed under the direction of Mr. Walter Shubert, Program Manager, and Messrs. Carl Ring and Robert Marable, Engineers.

PRECEDING PAGE BLANK NOT FILMED

CONTENTS

Section			Page
I	INTR	DDUCTION AND SUMMARY	1
II	DESIG	GN AND FABRICATION	3
	A.	Computer Code 5160	5
	В.	Computer Code 8272	13
	C.	Computer Code 8530	13
III	TEST		15
IV	TEST	RESULTS	23
	A.	Engine Performance	23
	B.	Heat Transfer Characteristics	30
ATTAC	CHMENT	1 — RL10 Derivative II Chamber/Primary Nozzle Low Cycle	
Fatigue	Report .		35
ATTAC	CHMENT	2 — Photographic Record of Fabrication	75
ATTAC	CHMENT	3 — Throat and Injector Face Prior to First Firing	101
		4 — Injector Face, Throat and Primary Nozzle Interior After	109
		5 — Injector Face, Combustion Chamber, and Throat After R 68.01	125

PRECEDING PAGE BLANK NOT FILMED



ILLUSTRATIONS

Figure		Page
1	RL10 Derivative II Nozzle Nomenclature — Computer Decks 5160-81, -92	(
2	Comparison of Coolant Flow Areas Between RL10A-3-3 and RL10 Derivative II	7
3	RL10 Derivative II Thermal Characteristics — O/F = 6.0	8
4	RL10 Derivative II Thermal Characteristics — O/F = 5.4	g
5	RL10 Derivative II Thermal Characteristics — O/F = 6.5	10
6	RL10 Derivative II 2-D Throat Heat Transfer Analysis — Axial Distance = -0.4 in., O/F = 6.0	11
7	RL10 Derivative IIB Comparison of Hot Wall Temperature Profiles from 1-D and 2-D Thermal Analyses	12
8	RL10 Derivative II Thermocouple Locations	17
9	RL10 Derivative II Thermocouple Locations	18
10	RL10 Derivative II Thermocouple Installation	19
11	Engine XR102-5 Mounted in E-6 Test Stand	20
12	Engine XR102-5 Mounted in E-6 Test Stand	21
13	RL10 Derivative II Engine Runs — Vacuum Specific Impulse vs Inlet Mixture Ratio	24
14	RL10 Derivative II Engine Runs — Chamber Pressure vs Inlet Mixture Ratio	26
15	RL10 Derivative II Engine Runs — Fuel Side Pressure Loss vs Chamber Mixture Ratio	27
16	RL10 Derivative II Engine Runs — Fuel Side Pressure Loss vs Chamber Mixture Ratio	28
17	RL10 Derivative II Engine Performance Plots	29
18	RL10 Derivative II Primary Nozzle Analytical and Test Data Comparison at O/F =5.4	31
19	RL10 Derivative II Primary Nozzle Analytical and Test Data Comparison at O/F = 6.0	32

ILLUSTRATIONS (Continued)

Figure		Pag
20	RL10 Derivative II Primary Nozzle Analytical and Test Data Comparison at O/F =6.5	3
21	Tube and Mae West Model Section	3
22	A Slice of the Model at a Plane Containing Integration Points	3
23	RL10 Nozzle Tube MARC 3-D Finite Element Model	3
24	Table 4 Data Headers	4
25	Node Transformation Boundary Conditions	4
26	RL10A-3-3 Transient MARC Heat Transfer Model	4
27	RL10A-3-3 Stress Model	4
28	RL10A-3-3A Heat Transfer Model With Braze in Throat	4
29	RL10 Derivative II — Sample Heat Transfer Data	5
30	RL10 Derivative II — Slice of the Model at a Plane Containing Integration Points	5
31	RL10 Derivative II — Thermal Data Overlaid Onto Integration Points	5
32	AISI 347 LCF Curves in Air	6
33	AISI 347 LCF Curves in Hydrogen Atmosphere — 1600°F	6
34	AISI 347 LCF Curves in Hydrogen Atmosphere — 1400°F	6
35	AISI 347 LCF Curves in Hydrogen Atmosphere — 1000°F	6
36	AISI 347 Tensile Strength vs Temperature	6
37	AISI 347 Tensile Ductility vs Temperature	6
38	AISI 347 Tensile Stress vs Strain	6
39	AISI 347 Tensile Stress vs Temperature and Plastic Strain	68
40	AISI 347 Elastic Modulus vs Temperature	70
41	Band Harness — RL10 Derivative II vs RL10A-3-3	7
42	Band Harness With Fixture Bands Installed	78

ILLUSTRATIONS (Continued)

Figure		Page
43	Band Harness and Mandrel Assembled for Curing	79
44	Long Tubes Stacked in Exit Manifold	80
45	Hooked Tube Exit Manifold Showing Sockets	81
46	Long Tube Stack Installed on Mandrel	82
47	Long Tube Stack on Mandrel With Retaining Hooks	83
48	Long Tube Stack Installed on Mandrel	84
49	Long Tube Stack Installed on Mandrel	85
50	Completed Stack With Short Tubes and Inlet Manifold Installed	86
51	Short Tubes and Inlet Manifold Installed	87
52	Reinforcing Band Segments Installed	88
53	Reinforcing Band Segments Installed With Welded Latches	89
54	Reinforcing Band Installation	90
55	Band Harness Installation	91
56	Completed Assembly Ready for Furnace Braze	92
57	Post-Braze Assembly After Removal From Furnace	93
58	Post-Braze Assembly After Removal From Furnace	94
59	Post-Braze Assembly After Removal From Furnace	95
60	Brazed Assembly After Removal From Mandrel	96
61	Primary Nozzle Interior	97
62	Combustor Chamber Interior Showing Hooked Tubes	98
63	Post-Braze Exit Manifold Tube Sockets	99
64	Chamber/Primary Nozzle — RL10 Derivative II vs RL10A-3-3	100

TABLES

Table		Page
1	Proposed Test Matrix	16
2	RL10-IIC Test Run Summary (Engine XR102-5)	23
3	RL10-IIB Predicted vs Actual Performance	25
4	Tube Data from Mechanical Design	42
5	Flight Point and Corresponding Increment in the 32 Increment Analysis	44
6	Tube Data from Mechanical Design	48
7	1400°F, Air Data	60
8	1600°F, Hydrogen Data	60
9	1400°F, Hydrogen Data	61
10	1000°F, Hydrogen Data	62
11	Tensile Data for PWA 770 (AISI 347 Stainless Steel Tube)	66
12	Tensile Stress-Strain Parameters for PWA 770 (AISI 347 Steel Tube)	69
13	Approximate Strain Ranges at Three Engine Conditions	73

PRECEDING PAGE BLANK NOT FILMED

SECTION ! INTRODUCTION AND SUMMARY

The design, fabrication, and test of the RL10-II chamber/primary nozzle was accomplished as part of the RL10 Product Improvement Program (PIP). The overall goal of the RL10 PIP was to gain the knowledge and experience necessary to develop new cryogenic upper stage engines to fulfill future NASA requirements. The goal would be reached by producing an RL10 engine designed to be reusable, operable at several thrust levels, and have increased performance. The goals for the chamber/primary nozzle task were to design a reusable assembly capable of operation at increased mixture ratio and low thrust, fabricate three assemblies using new or updated techniques where possible, and test one assembly to verify the design and construction.

The goals for the chamber/primary nozzle task were realized satisfactorily.

The design phase produced an assembly having improved features such as single-piece reinforcing band (Mae West) segments and relocated tube exit braze joints (hooked tube). In addition, a computer program was developed to design the chamber tubes to meet both performance and heat transfer requirements.

The fabrication phase made use of the new Mae West design to procure cold-formed segments which contained no welds, were free of cracks, and required fewer pre-braze operations when compared to the existing production engine design. The single-piece Mae West segment has since been incorporated into the RL10A-3-3A. A casting was used to fabricate the "hooked tube" exit manifold. This reduced the total cost as compared to a fully machined manifold. Inhouse operations were reviewed and made more efficient, and these improvements were incorporated into the production engine processes.

The test phase showed the chamber/primary nozzle performance to be as predicted. These results, along with the heat transfer data obtained, proved the overall design of the RL10-II chamber/primary nozzle.

Included in this report are the Low Cycle Fatigue Analysis Report (Attachment 1), a photographic record of the fabrication (Attachment 2), and photographic records of the testing (Attachments 3, 4, and 5).

SECTION II DESIGN AND FABRICATION

The design of the RL10 Derivative II chamber and primary nozzle was based on experience gained during the design of the RL10A-3-3 thrust chamber. The assembly was designed to have an overall shorter length than the RL10A-3-3, and a service life of 10 hours/180 cycles. The combustion chamber length was increased to make up for the reduction in heat transferred to the coolant from the shorter primary nozzle. The lengths of the combustor chamber and primary nozzle are 15 inches and 30 inches respectively. The throat diameter was also reduced from 2.57 inches for the RL10A-3-3 to 2.472 inches for the Derivative II engine. The maximum predicted hot wall temperature was reduced to 100°R less than the RL10A-3-3B maximum hot wall temperature to meet the 10 hour/180 cycle low cycle fatigue (LCF) life established for the RL10 Derivative II engine.

The chamber/primary nozzle is a pass and one-half tubular design similar to the RL10A-3-3. There are 180 short and 180 long tubes brazed together circumferentially to form the nozzle. There also is a turnaround manifold, fuel inlet manifold, fuel exit manifold, and various stiffeners and component supports which are nearly identical to the RL10A-3-3 components. The two main functions of the chamber/primary nozzle are to provide a converging-diverging design for the combustion and acceleration of propellants, and to serve as a heat exchanger to supply turbine power for the propellant pumps. The inlet and exit manifold relative positions were unchanged so that the current turbopump and plumbing would fit without modification.

The nozzle inner contour is determined from a combustion analysis and a spline-fit computer program that will provide a smooth and continuous nozzle inner contour. A computer program was developed to determine the internal flow area of the tubes based on heat transfer flow requirements and tube geometry.

High coolant pressure inside the tube, along with the large temperature gradient between the hot wall and the cold wall on the combustion side of the tube, produces large plastic strains on the surface of the hot wall, limiting the LCF life of the hot wall. The LCF life analysis is described in detail in Attachment 1. At the conditions predicted by the heat transfer and stress analyses, the predicted LCF life is 230 cycles.

The minimum tube diameter located at the throat is the same as the RL10A-3-3. This is determined by the amount of pressure drop that is acceptable to maintain turbopump efficiency.

The inlet manifold is the same as the RL10A-3-3 except for the attaching hardware that is modified to match the new nozzle contour.

The exit manifold features a "hooked tube" design. This design places the braze joint inside the manifold and away from the hot wall. Previous testing on the present RL10 configuration at low thrust conditions produced sufficient temperature gradients diametrically across the joint to cause cracking in the braze joint. The "hooked tube" configuration was designed and successfully tested during development of the RL10A-3-7 engine.

The tubes that are brazed together to form the nozzle are structurally supported by stiffener bands designed to carry 100 percent of the chamber hoop loads. These bands also minimize the effect of any flow-induced vibration.

The two gimbal actuator attachment points are part of the fuel inlet manifold. They are essentially the same as the present RL10 except for the actuation angle. This angle was changed to allow for clearance between the actuator rod and the retracted secondary nozzle. The

maximum actuator load is 2640 pounds. This is the current Centaur vehicle actuator load limit during gimballing. Shear stresses at the welds are 35 percent below the allowable stresses.

The turbopump mounting struts required a slight angle change from the present RL10 to facilitate mounting on the new nozzle contour. This change was designed to have a minimum effect on the structure stiffness and load carrying capacity.

Fabrication of all three chamber/primary nozzle assemblies was completed without significant difficulty. A photographic record of the fabrication of the first assembly is provided in Attachment 2.

The thermal analysis of the RL10 Derivative IIB chamber/primary nozzle consists of a one-dimensional (1-D) and more detailed two-dimensional (2-D) thermal analysis. The analysis was accomplished by using computer codes 5160, 8272, and 8350. The 1-D thermal analysis was performed using the 5160 program, which is a modularized rocket heat transfer and flow program. Two specialized versions of deck 5160 were used in the analysis. Computer codes 5160-92 and 5160-81 have been set up to model tubular heat exchangers. The 5160-92 code is further specialized to model the chamber and single pass section of the primary nozzle. The 5160-81 code is specialized to model the primary nozzle with a pass and a half coolant jacket. Figure 1 shows a diagram of the RL10 derivative IIB chamber/primary nozzle with nozzle nomenclature, computer codes used, and geometry data required by the computer programs. Computer code 5160 is covered in more detail in a later section.

The RL10 Derivative IIB chamber cooling jacket was designed during the 1-D analysis with a maximum wall temperature of 2177°R at the design point of 6.0 mixture ratio. This wall temperature is 100°R below the normal operating temperature of the RL10A-3-3B. A reduction of 200°R in wall temperature was attempted during the early part of the analysis but resulted in unacceptably high coolant jacket pressure drop. The pressure drop in the jacket was minimized by limiting coolant Mach number to 0.55 and by limiting the minimum coolant passage area to 0.006 in.2. These limits were also used in the design of the RL10A-3-3. Figure 2 shows a comparison of the coolant passage flow areas between the RL10 Derivative IIB and RL10A-3-3. The coolant passage flow areas upstream of the throat in the chamber were reduced compared with the RL10A-3-3 where heat flux is high. In the nozzle, the heat flux to the wall is low so that coolant passage area has been increased compared with the RL10A-3-3. Figure 3 shows the 1-D thermal analysis results of the RL10-IIB at the design point mixture ratio of 6.0 and 15,000 pounds thrust. The maximum hot wall temperature of 2177°R, resulting in a tube temperature margin of 437°R, occurs near the throat. Tube temperature margin is the difference in temperature between the tube operating temperature and the material temperature limit at the operating stress. The coolant which enters the jacket at 58°R and 852 psia has a temperature rise of 374°R and a pressure drop of 155 psi. Figures 4 and 5 show the 1-D thermal analysis results for the off-design O/F points of 5.4 and 6.5. The maximum hot wall temperatures at the O/F ratios of 5.4 and 6.5 are 1980°R and 2350°R respectively. The coolant temperature rise at 5.4 and 6.5 mixture ratios is 332.5°R and 628°R, while the coolant pressure drop is 158 psi and 142 psi, respectively.

The 2-D thermal analysis was accomplished with computer codes 8272 and 8530. Deck 8272 is a P&W developed general heat transfer program. The 2-D thermal analysis was done to investigate the effects of conduction, through and around the coolant tube wall, on the hot wall surface temperature. The 2-D analysis was done only near the throat where local heat flux and hot wall temperatures are highest. The geometry factors and major boundary conditions from deck 5160 were used in the 2-D thermal analysis. The geometry information from deck 5160 was used by deck 8530 to create the finite difference quadrilateral mesh used by deck 8272. The heat flux through the hot wall in the 2-D thermal model has been set to the heat flux calculated by

deck 5160. The accuracy of this heat flux has been verified in past RL10 testing. Figure 6 shows the 2-D temperature predictions for the coolant jacket tube wall at a position 0.4 inch upstream of the throat. These temperatures are the maximum wall temperatures at the design point of 6.0 mixture ratio (MR). The effects of the conduction mechanism in the 2-D analysis can be seen by the fact that the maximum hot wall surface temperature prediction of 2101°R is 87°R cooler than previously predicted in the 1-D analysis. The tube wall conduction effects are stronger at the throat where tube perimeters are small compared with the wall thickness. The 2-D hot wall temperature profile starting 1.0 inch upstream of the throat and ending 1.0 inch downstream of the throat can be found in Figure 7.

COMPUTER CODE 5160

Deck 5160 is a modularized rocket heat transfer and flow program. Computer decks 5160-92 and 5160-81 are specialized versions set up to model tubular coolant jackets. Deck 5160-92 has been set up to model the single pass chamber and nozzle. Deck 5160-81 has been set up to model the double pass section of the nozzle.

Deck 5160 uses the Mayor integral with enthalpy driving potential to define the combustion side heat transfer environment. Combustion properties are built into the deck. Heat flux calculations in deck 5160 are based on enthalpy instead of temperatures. The heat flux equations in D5160 are shown below.

H×EDP/CP Heat flux =

Heat transfer film coefficient Enthalpy driving potential EDP

CP Specific heat.

The enthalpy driving potential is equal to the change in enthalpy from the free stream to the wall. The enthalpy driving potential is equal to the following.

 $\rm h_o$ - $\rm h_{wall}$ - (1– $\rm P_r^{\,0.333})dhk$ (kinetic energy term) Free stream stagnation enthalpy

Enthalpy at wall Prandtl number

Change in enthalpy due to kinetic energy.

The free stream stagnation enthalpy is calculated at the injector and is held constant throughout the length of the chamber and nozzle. The enthalpy at the wall is equal to:

 h_{ref} - $(T_{ref}$ - $T_{wall})$ cp Reference temperature Reference enthalpy Specific heat.

The reference and stagnation enthalpies are based on the heat recovered at the wall due to chemical reactions of the dissociated combustion products. Rocket combustion products are dissociated at temperatures above 2700°R and recombine and release heat at low temperatures near the wall. Diffusion of these dissociated combustion products into the boundary layer will enhance effective conductivity and enthalpy driving potential. The reference temperature in the above equation is usually set to 2700°R with its respective enthalpy. The free stream stagnation enthalpy includes the enhancement due to total recombination of the combustion products,

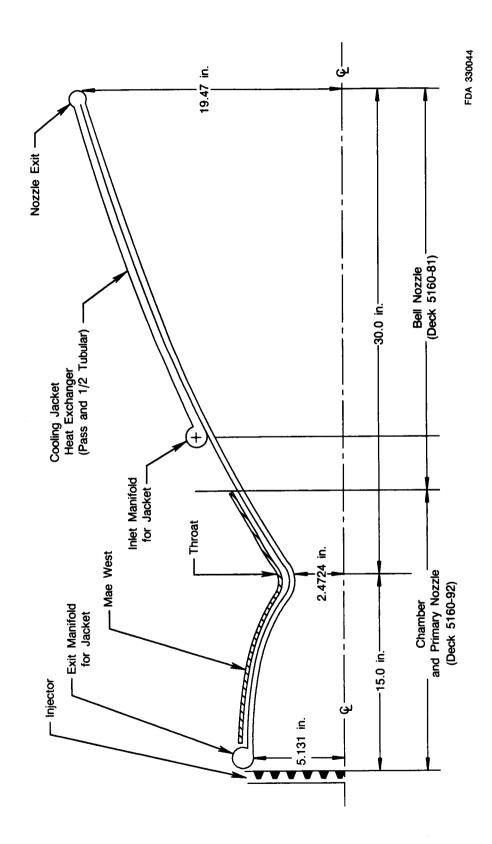


Figure 1. RL10 Derivative II Nozzle Nomenclature — Computer Decks 5160-81, -92

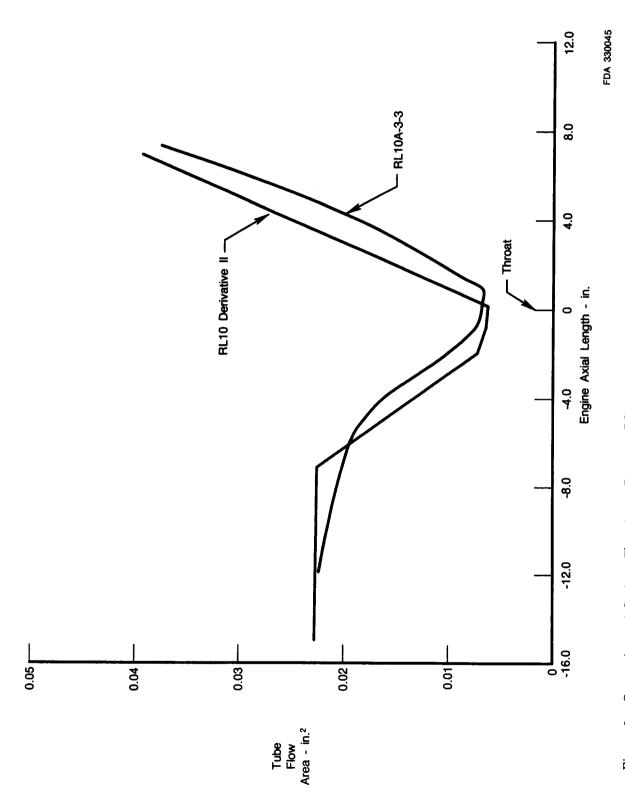


Figure 2. Comparison of Coolant Flow Areas Between RL10A-3-3 and RL10 Derivative II

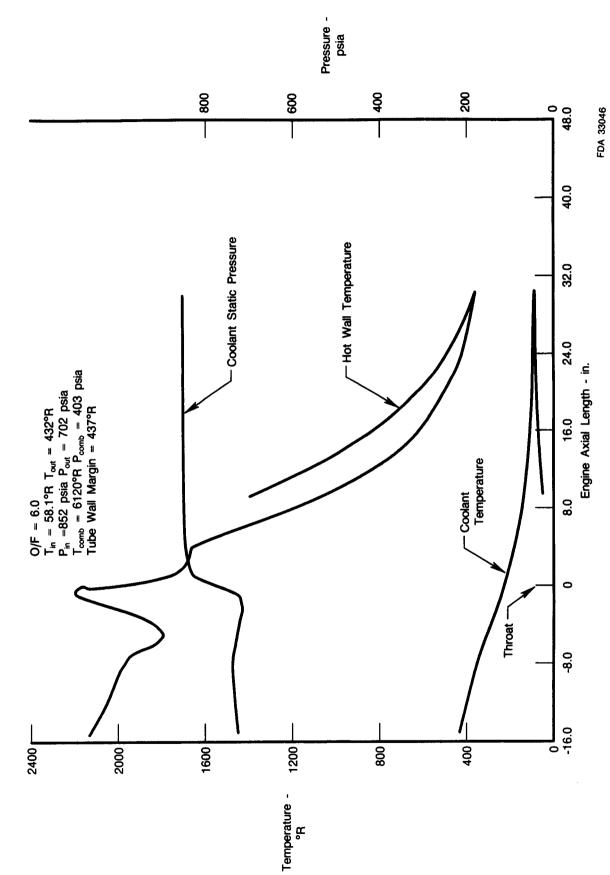


Figure 3. RL10 Derivative II Thermal Characteristics — 0/F = 6.0

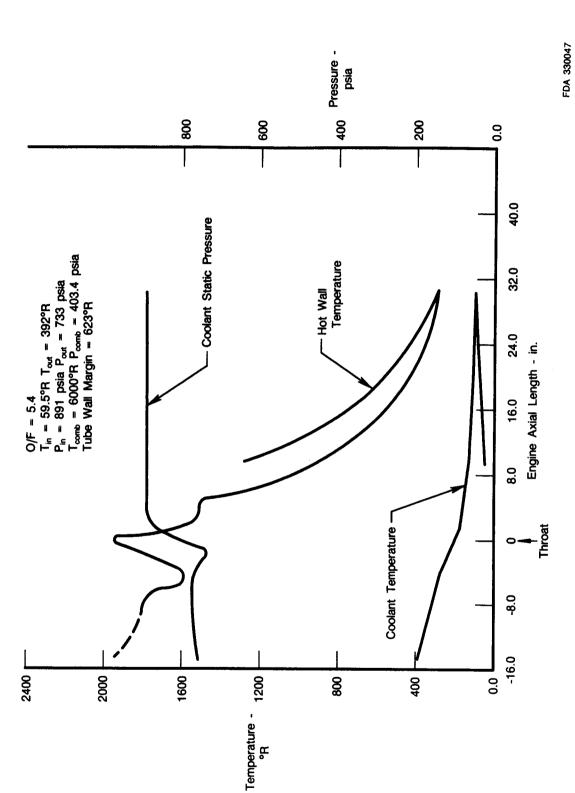


Figure 4. RL10 Derivative II Thermal Characteristics — 0/F = 5.4

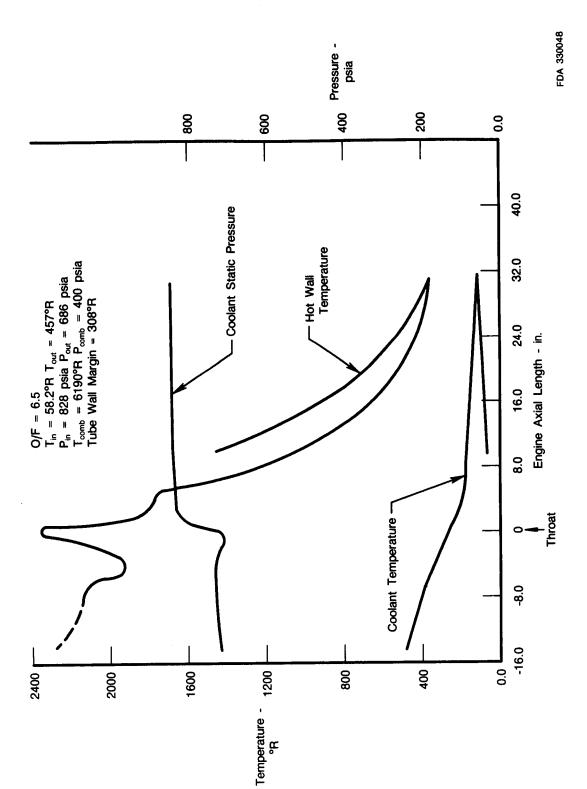
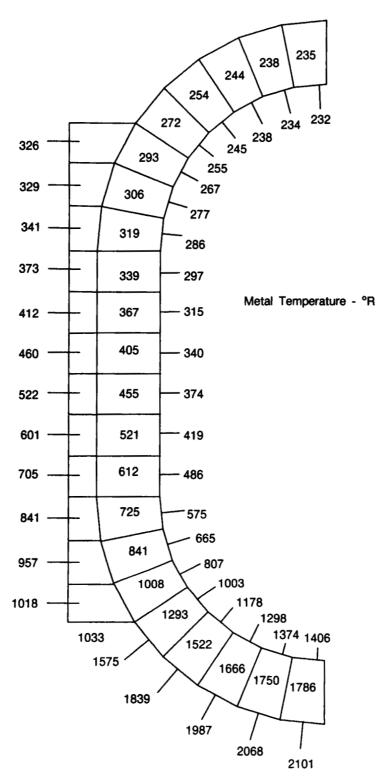


Figure 5. RL10 Derivative II Thermal Characteristics — O/F = 6.5



FDA 330049

Figure 6. RL10 Derivative II 2-D Throat Heat Transfer Analysis — Axial Distance = -0.4 in., O/F = 6.0

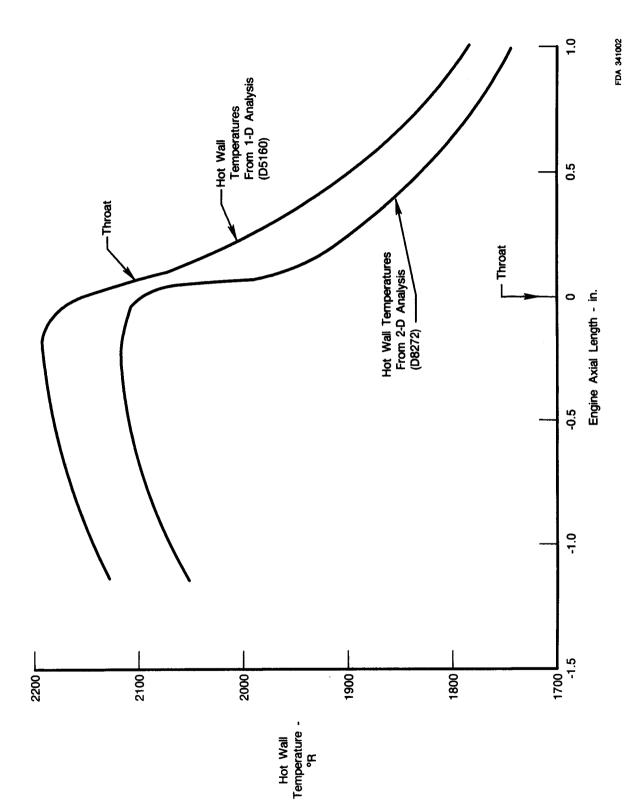


Figure 7. RL10 Derivative IIB Comparison of Hot Wall Temperature Profiles from 1-D and 2-D Thermal Analyses

The hydrogen coolant side heat transfer film coefficients are based on the modified Dittus-Boelter equation. The equation has been modified for density variations from the balk to film temperature. The coolant side heat transfer film coefficient is automatically corrected for passage surface roughness and passage curvature.

B. COMPUTER CODE 8272

Computer code 8272 is a P&W developed generalized heat transfer program that was used to evaluate 2-D heat transfer aspects of the RL10 Derivative II chamber and nozzle. This program has the capability of solving for the temperature distribution for any irregular shaped two or three dimensional object by dividing it into the desired number of nodes. The program allows the user to calculate both transient and steady-state temperatures as a function of various input parameters.

A heat balance equation accounting for conduction, convection, radiation, internal heat generation, and heat storage is written for each node. For steady-state solutions, the heat storage is set to zero and the model equations are solved simultaneously by matrix inversion using a band type solution. Iteration is necessary when radiation terms are introduced or when a property is considered dependent on the resultant temperature. A successive substitution method of iteration is used until a specific degree of tolerance is established.

For transient solutions, a forward difference technique is employed where the temperature at time $\Theta + \Delta\Theta$ is a function of the temperature and properties at time Θ . The size of the time increment, $\Delta\Theta$, determines the stability and convergence of the solution.

Numerous user convenience factors have been incorporated into the program. Some of these are built-in properties, internal geometry subroutines, internal film coefficient calculations, and fluid heat-up capabilities.

C. COMPUTER CODE 8530

Computer code 8530 is a P&W developed program that creates the finite difference quadrilateral mesh that defines the geometric shape to be evaluated by computer code 8272. The quadrilateral mesh contains the geometric information such as node volumes, conduction lengths, conduction areas, the convection areas needed in computer code 8272. The geometric mesh can be created for any 2-D irregular shape. The geometric shape can be input into 8530 as a digitized cross section.

SECTION III TEST

A test matrix was formulated to verify the heat transfer analysis and performance characteristics of the chamber/primary nozzle. The test matrix is shown in Table 1.

In addition to the standard engine instrumentation, thermocouples were installed on the nozzle tubes on both the interior and exterior of the nozzle. Figures 8, 9, and 10 show the thermocouple installation. Two rows of six locations were chosen along the nozzle that were considered the minimum required to determine the temperature profile. Thermocouples were installed at each location, one on the hot wall and one on the outside wall. It is not feasible to place thermocouples in the combustion chamber because of the very high heat fluxes; the thermocouple and wires would not survive the severe environment.

RL10 development engine XR102-5 was built as an RL10-IIC using the first chamber/primary nozzle S/N BKW600. Only two problems were encountered during engine build requiring rework. One turbopump support bracket was mislocated, leaving a gap between the bracket and the turbopump housing. A spacer was made to fill this gap. The second problem was the turbine discharge line could not be installed because of an interference between the nozzle surface and the horizontal section of the line. The line was heated and reformed to allow installation.

The engine was mounted in the E-6 altitude test facility as shown in Figures 11 and 12. A water cooled exhaust deflector was built to direct the exhaust from the shorter engine into the diffuser. It can be seen directly below the nozzle exit. The condition of the chamber/primary nozzle interior prior to the first firing is photographically documented in Attachment 3.

The first test, HR 65.01, was a normal firing of 400 seconds duration. During the test the engine was trimmed to 403 psia chamber pressure (P_c) at 5.0:1 mixture ratio (MR). Mixture ratio was then varied over a range from 4.4 to 5.6. The chamber/primary nozzle condition was excellent after the test, as shown in Attachment 4. The hotside thermocouples were lost at the beginning of the run, apparently due to lack of protecting braze around the thermocouple sheaths. The sheaths were spot brazed to the coolant tubes instead of continuously brazed, which did not provide adequate cooling of the sheath.

The second test, HR 66.01, was run for 350 seconds. Engine trim was attempted at 443 psia P_c and 5.0 MR; however, the engine was out of power at 5.0 MR and P_c would not go above 440 psia. This was a result of trying to increase P_c at a constant MR, thereby requiring more work from the pumps without increasing the available energy to the turbine. Mixture ratio was again varied from 4.4 to 5.6. The interior of the chamber/primary nozzle continued to look good.

The next two tests were to be run at 6.0:1 MR. This required a smaller fuel pump discharge orifice diameter, so the standard Class 1 orifice was removed and a Class 4 orifice was installed.

The third test, HR 67.01, was run for 375 seconds. The engine was trimmed at 403 psia P_c and 6.0:1 MR. This is the design point for the RL10-IIC. Mixture ratio was varied from 5.4 to 6.6. The chamber/primary nozzle did not show any deterioration due to the increase in mixture ratio.

Table 1. Proposed Test Matrix

		Remarks	41.0±1.0 Trim to P _c =403 psia and 5.0 MR, P-U excursion and check for power margin.	41.0 ± 1.0 Trim to $P_c = 443$ psia and 5.0 MR, P-U excursion.	41.0±1.0 Trim to P _c =403 psia and 6.0 MR, P-U excursion and check for power margin.	41.0±1.0 Trim to P _c =443 psia and 6.0 MR, P-U excursion.
	OPIP	(psia)	41.0±1.0	41.0 ± 1.0	4 1.0 ± 1.0	1
te Inlets	OPIT	(°R)	176.0 ± 2.0	176.0 ± 2.0	176.0 ± 2.0	176.0±2.0
Steady-State Inlets	FPIP	(psia)	25.0 ± 0.65	38.5±0.5 25.0±0.65	25.0 ± 0.65 176.0 ± 2.0	38.5±0.5 25.0±0.65
	FPIT	(°R)	38.5 ± 0.5	38.5 ± 0.5	38.5 ± 0.5	38.5 ± 0.5
tart	(c)	XOT	220	220	220	220
Prestart	(sec)	Fuel	40	40	40	40
	OPIP	(psia)	44.0±1.0	44. 0±1.0	44.0±1.0	44.0±1.0
Inlet	OPIT	(R)	176.0±2.0	176.0 ± 2.0	176.0 ± 2.0	176.0±2.0
Start Inlet	rara	rrir (nsia)	27.5±0.5	27.5±0.5	27.5±0.5 176.0±2.0	27.5 ± 0.5
	Figure	rPII (9R)	38.5±0.5	38.5 ± 0.5	38.5 ± 0.5	38.5 ± 0.5
	i	Mo	1	63	က	4

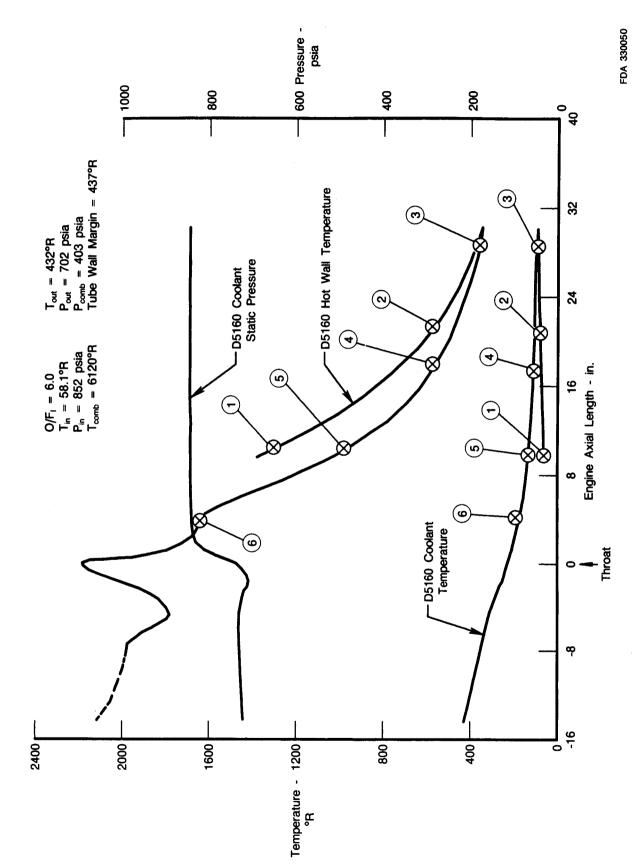


Figure 8. RL10 Derivative II Thermocouple Locations

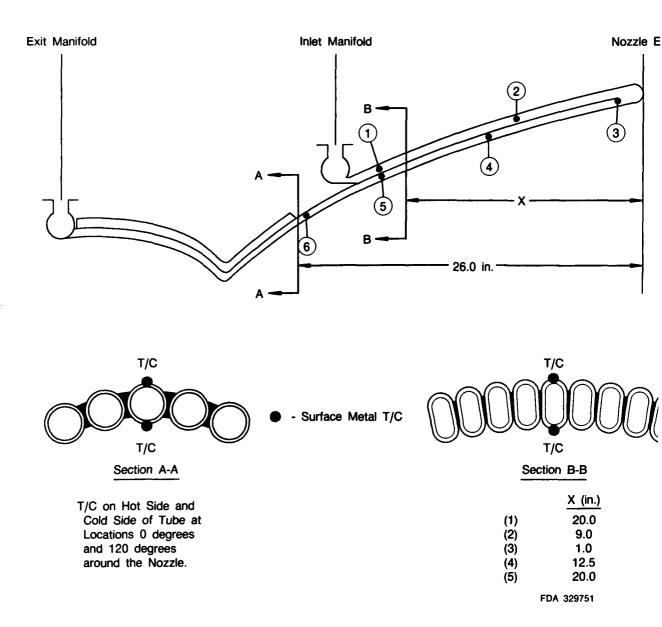
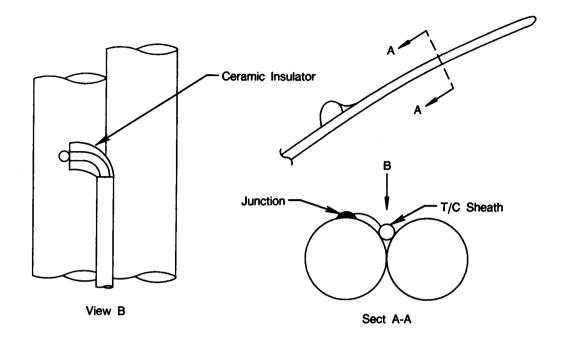


Figure 9. RL10 Derivative II Thermocouple Locations

The fourth and final test, HR 68.01, was run for 310 seconds. The desired engine trim point was 443 psia P_c and 6.0 MR. Mixture ratio was varied from 5.4 to 6.6 and the engine ran out of power at 5.8 MR. Below this mixture ratio, a P_c of 443 psia could not be maintained, as in HR 66.01.

The engine was pulled and the chamber/primary nozzle was thoroughly inspected. The hardware was in excellent condition, as shown in Attachment 5. One small leak was found adjacent to the turnaround manifold at the nozzle exit where a thermocouple was mounted and had burned away.

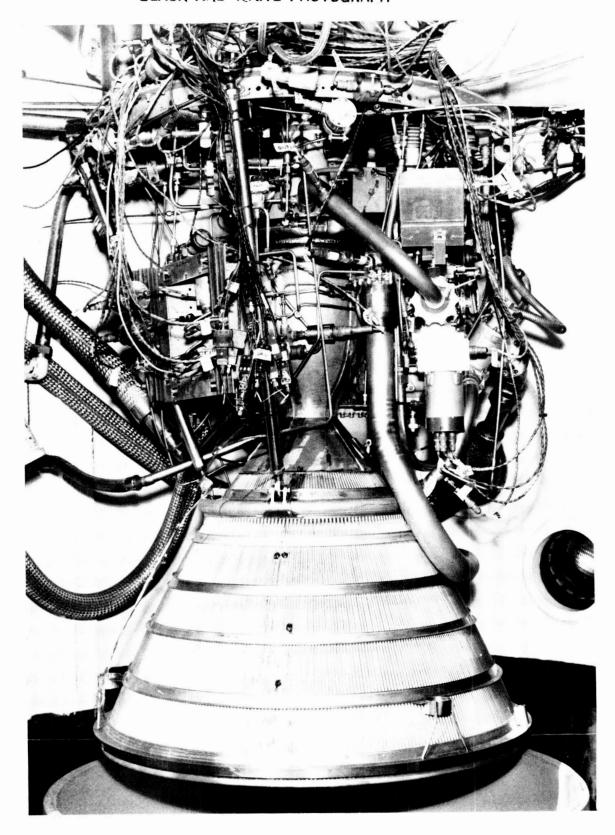


FDA 329752

Figure 10. RL10 Derivative II Thermocouple Installation

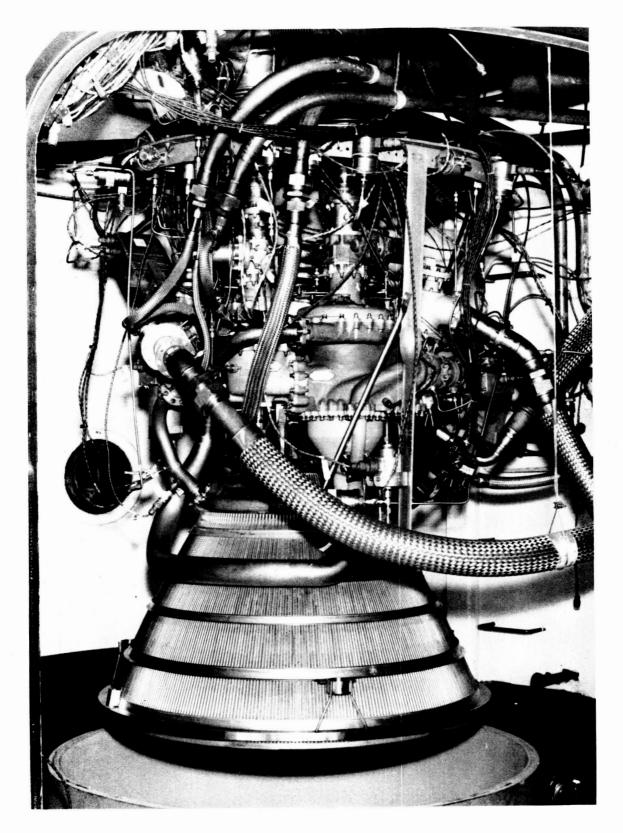
ţ

ORIGINAL PAGE BLACK AND WHITE PHOTOGRAPH



FE360514-2

Figure 11. Engine XR102-5 Mounted in E-& Test Stand



FE 360514-5

Figure 12. Engine XR102-5 Mounted in E-6 Test Stand

SECTION IV

Total run time for this build was 1435.1 seconds. Engine performance is summarized in Table 2.

Table 2. RL10-IIC Test Run Summary (Engine XR102-5)

			Test Date			
Item		Units	3-19-86	3-20-86	3-21-86	3-21-86
Run No.			65.01	66.01	67.01	68.01
Run Duration		sec	400.1	350.0	375.1	309.9
Accumulated Hot Time		sec	400.1	750.1	1125.2	1435.1
Prestart Duration Fuel/LOX		sec	45/250	45/250	45/250	45/250
OPIP Prestart/Start		psia	42.8/44.2	51.1/51.5	43.9/44.2	44.1/44.3
OPIT Prestart/Start		°R	176.2/175.8	176.1/175.8	176.3/175.9	175.7/175.5
FPIP Prestart/Start		psia	27.7/27.5	28.0/28.0	27.5/27.4	27.5/27.4
FPIT Prestart/Start		°R	38.8/38.3	38.9/38.4	38.4/38.0	38.7/38.2
OPHT Prestart/Start		°R	459/185	453/184	432/186	445/184
FPHT Prestart/Start		°R	461/52	453/51	421/54	433/51
FTIT Prestart/Start		°R	516/506	516/515	478/471	496/491
Time to Accelerate	(uncorrected)	sec	1.603	1.678	1.717	1.738
STIMP to 3 sec	(uncorrected)	lb/sec	21,726	22,466	19,551	21,566
Sparks to Light			1	1	2	2
GMRV Cracking Pressure		psid	79	78	79	79
Min Static NPSP Fuel/LOX		sec	0.67/0.79	0.09/3.38	3.80/0.72	1.98/1.04
GMRV Cracking		sec	1.321	1.356	1.400	1.396
GOX to LOX		sec	1.500	1.530	1.579	1.575
Decel Time		sec .	0.141	0.144	0.131	0.134
Steady-State Thrust		lb	13,811	15,028	14,044	15,230
Steady-State Mixture Ratio			5.102	4.960	5.971	5.799
Steady-State Impulse		sec	421.7 at 5.0	423.2 at 5.0	416.9 at 6.0	417.5 at 6.0

16904

A. ENGINE PERFORMANCE

Specific impulse performance for the Derivative II chamber/primary nozzle assembly is presented in Figure 13 over the range of inlet mixture ratios (MR) tested. Inlet mixture ratio is the ratio of oxidizer pump to fuel pump flowrates. Specific impulse at 5.0 MR was within an average of 0.35 percent of the predicted values (as shown in Table 3). Specific impulse for the 6.0 MR case was within an average of 0.12 percent of the predicted values. The engine ran out of power at the low mixture ratio due to insufficient power to the turbine. The power limiting MRs for the high chamber pressure tests (Run 66.01 and Run 68.01) were 5.3 and 5.8, respectively and, as shown in Figure 14, the vented thrust control line for Run 68.01 is shifted, compared to Run 66.01. This is a result of the fuel pump discharge orifice change to a smaller diameter for Run 68.01.

Pressure loss and temperature rise characteristics for the chamber/primary nozzle are shown in Figures 15 and 16, respectively. Chamber mixture ratio is the ratio of oxidizer flowrate to fuel flowrate as injected into the combustion chamber. Comparison of actual to predicted values for Jacket Temperature Rise and Jacket Pressure Loss are shown in Table 3.

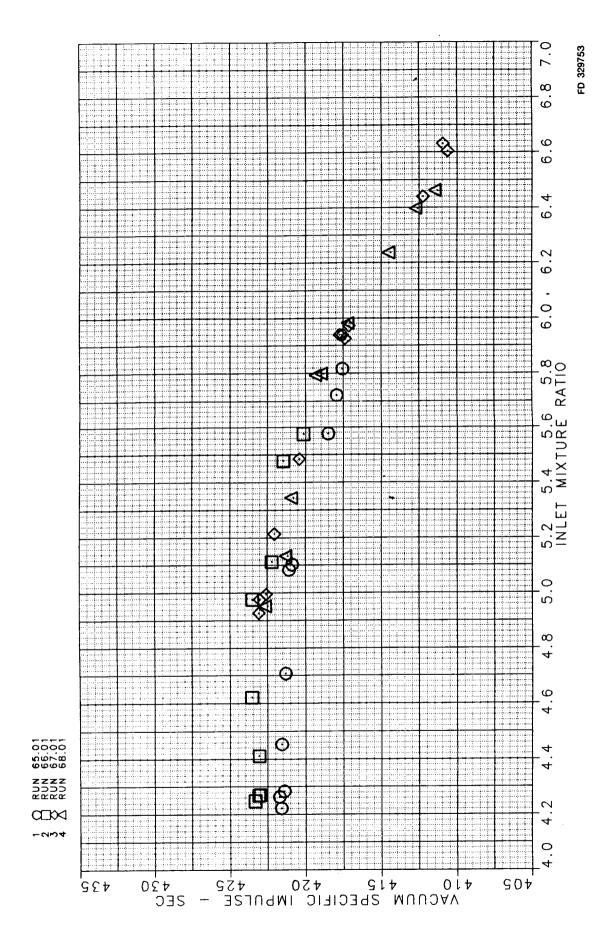


Figure 13. RL10 Derivative II Engine Runs — Vacuum Specific Impulse vs Inlet Mixture Ratio

Table 3. RL10-IIB Predicted vs Actual Performance

	Inlet Mixture	Chamber Pressure	Jacket Temp Rise (°R)		Jacket Press Loss (Tot) (psi)		Specific Impulse (sec)	
Run No.	Ratio	(psia)	Predicted	Actual	Predicted	Actual	Predicted	Actual
65.01	5.00	403.0	301.0	300.0	179.0	174.0	423.5	421.7
66.01	5.00	443.0	298.0	281.0	191.0	183.0	424.3	423.2
67.01	6.00	403.0	356.0	348.0	156.0	161.0	416.4	416.9
68.01	6.00	443.0	349.0	332.0	166.0	167.0	417.0	417.5

1629C

The high chamber pressure runs exhibited a "flatter" jacket pressure loss characteristic than the low chamber pressure runs (see Figure 16). This is most likely due to the fact that during the high chamber pressure runs, the engine was operating along the vented thrust control line.

Chamber performance characteristics, calculated from the test data, are shown in Figure 17 for the range of inlet mixture ratios tested. The parameters, thrust coefficient efficiency, impulse efficiency, and characteristic velocity efficiency, display the expected trends for an RL10 type engine for the tested mixture ratio range.

Figure 14. RL10 Derivative II Engine Runs — Chamber Pressure vs Inlet Mixture Ratio

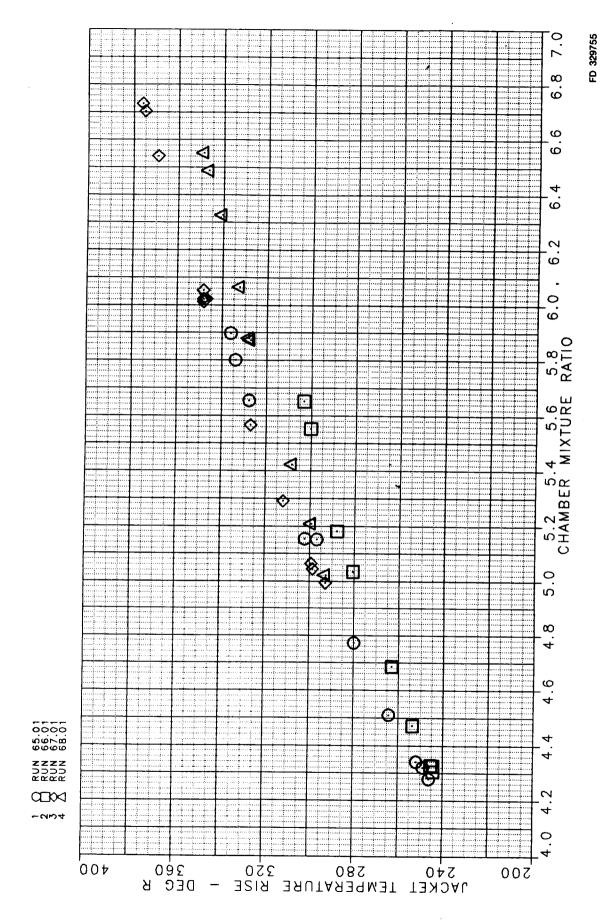
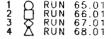
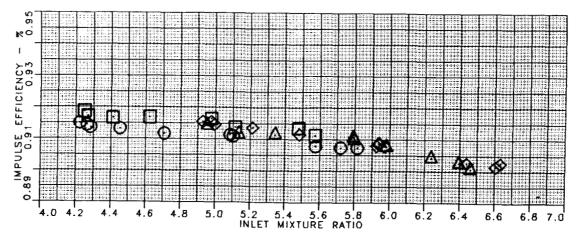


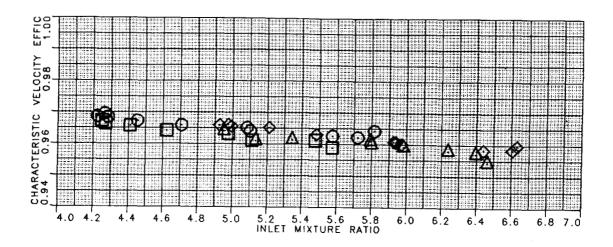
Figure 15. RL10 Derivative II Engine Runs — Fuel Side Pressure Loss vs Chamber Mixture Ratio

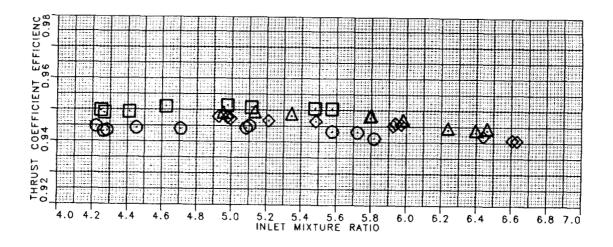
Figure 16. RL10 Derivative II Engine Runs — Fuel Side Pressure Loss vs Chamber Mixture Ratio

FD 329756









FD 329757

Figure 17. RL10 Derivative II Engine Performance Plots

B. HEAT TRANSFER CHARACTERISTICS

Figures 18, 19, and 20 compare test data with the analytical thermal model. The test data comparison lists the experimentally measured coolant temperature rise and pressure drop as well as its analytically predicted values. The figures also show the analytical and experimental cold wall temperatures. Hot wall temperatures were excluded because the thermocouples were lost. The comparisons have been made for mixture ratios of 5.4, 6.0, and 6.5. Based on the test data comparison, the thermal model of the RL10 Derivative IIB primary nozzle matches the test data closely.

The test data of the RL10 Derivative IIB primary nozzle coolant jacket shows close correlation between the test data and analytical thermal model. The comparison was made between the thermal model results and nominal or average test data results. The experimental coolant temperature rise and pressure drop data was also corrected for differences between the actual coolant flowrates and pressures, and those used in the analytical analysis. The thermal model coolant temperature rise across the jacket matches the nominal experimental data to within 9°R for all mixture ratios. The analytically determined coolant pressure drop matches the nominal test data within 1 psi. Actual coolant temperature rise and pressure drop test data was observed to vary around the analytically determined value due to engine run variations and also circumferential gas path temperature variations. The observed variations in the test data are approximately ± 3 percent in coolant temperature rise and ± 8 percent in coolant pressure drop.

Cold wall temperature data was compared to the predicted coolant temperature because cold wall temperatures are not generated by the thermal analysis. The cold wall temperature is hotter than the coolant because of conduction around the tube walls from the hot side to the cold side. The difference between the cold wall temperature and coolant temperature is greatest where coolant heat transfer film coefficients are low. High coefficients help to transfer heat out of the walls before it can reach the cold wall. At the end of the nozzle where the coolant heat transfer film coefficients are low, the cold wall temperature test data is 40°R higher than the coolant. At 4.0 inches from the throat where the coolant heat transfer is high, the cold wall data matches analytical coolant temperature within 10°R.

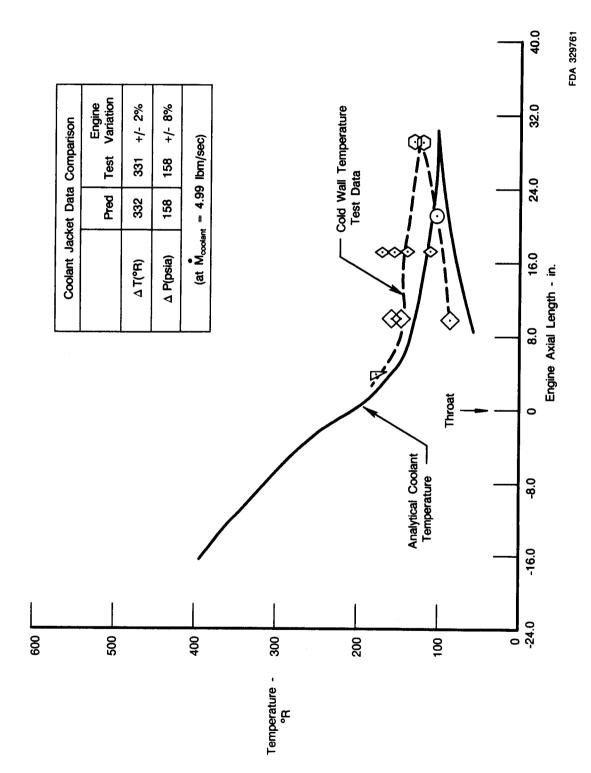


Figure 18. RL10 Derivative II Primary Nozzle Analytical and Test Data Comparison at O/F = 5.4

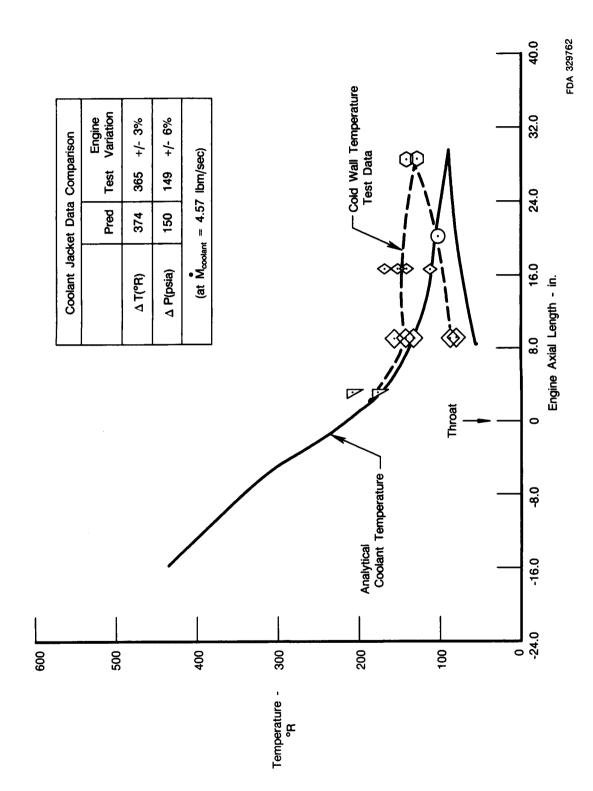


Figure 19. RL10 Derivative II Primary Nozzle Analytical and Test Data Comparison at O/F = 6.0

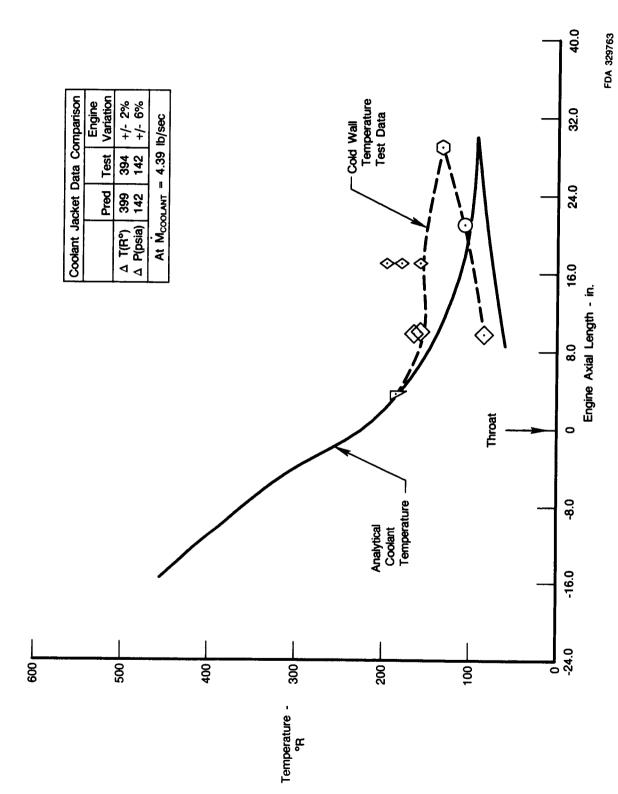


Figure 20. RL10 Derivative II Primary Nozzle Analytical and Test Data Comparison at O/F = 6.5

ATTACHMENT 1 RL10 DERIVATIVE II CHAMBER/PRIMARY NOZZLE LOW CYCLE FATIGUE REPORT

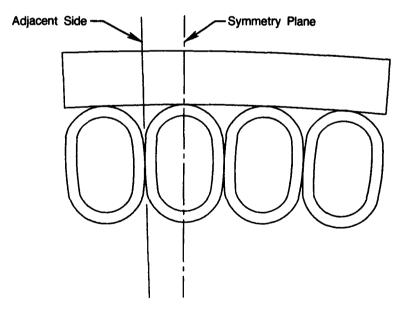
PRECEDING PAGE BLANK NOT FILMED

RL10-II

The analysis of the RL10-II chamber/primary nozzle resulted from a product improvement program for the RL10 rocket engine, in which the RL10-II is a reusable application. When compared to the RL10A-3-3, the Derivative II has a reduced throat area, a larger area ratio $(A_{\rm exit}/A_{\rm throat})$, a longer combustion chamber, a shorter primary nozzle, and an extendible secondary nozzle. The chamber/primary nozzle section is constructed of 360 PWA 770 (AISI 347) stainless steel tubes, which are brazed together. It is the LCF life of these tubes that is the concern of this analysis.

Because of the large temperature range $(-300^{\circ}\text{F} \text{ to } 1700^{\circ}\text{F})$ experienced in this problem, it was decided to use MARC (T793), a nonlinear 3-D finite element deck, to do an elastic-plastic analysis to determine a strain range. This strain range is then used to calculate an LCF life. One flight cycle was modeled and consisted of five flight conditions; cryogenic pre-ignition, tank head idle, pumped idle, full thrust, and shutdown. It was the strain range generated by this cycle that was used in the LCF calculation.

The loads for this problem were thermal and pressure loads and were generated by the heat transfer analysis. The thermal loads were output from Deck 8272 and the pressure loads were output from Deck 5160. The thermal loads were given at five axial locations and for the following conditions: cryogenic pre-ignition, tank head idle, pumped idle, full thrust, and shutdown. From the heat transfer analysis, the hottest spot in the chamber/nozzle was determined to be 0.4 inch in front of the throat (towards the injector). A finite element model of half of a tube and corresponding segment of Mae West was constructed spanning a distance from one inch in front of the hot spot to one inch behind the hot spot. The large thermal gradients dictated a finer breakup on the bottom of the tube and in the area of the hot spot (Figures 21, 22, and 23).



FDA 329764

Figure 21. Tube and Mae West Model Section

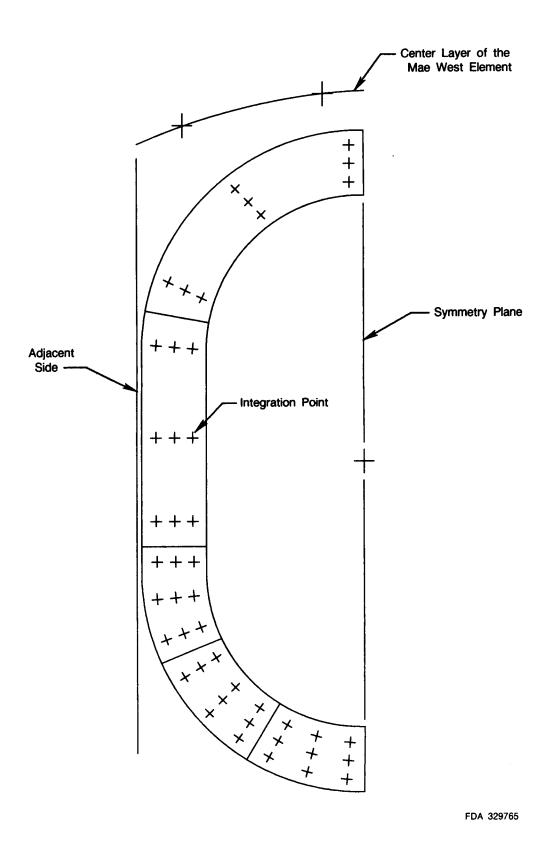


Figure 22. A Slice of the Model at a Plane Containing Integration Points

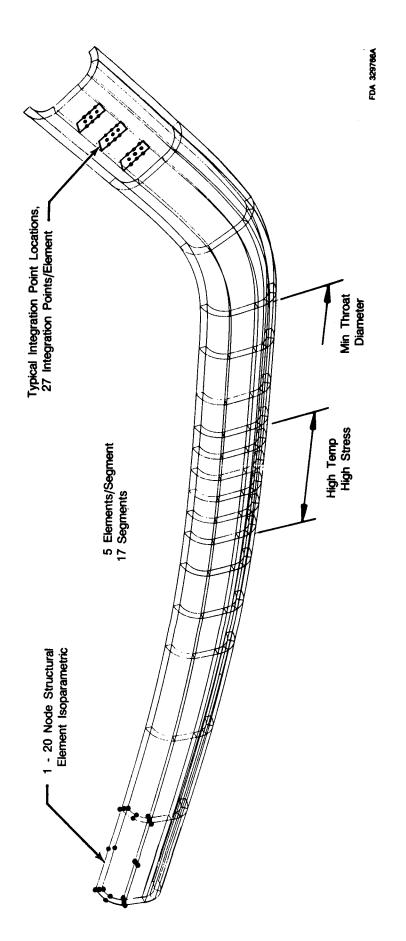


Figure 23. RL10 Nozzle Tube MARC 3-D Finite Element Model

The structural model consisted of 102 elements, 85 twenty-node brick elements for the tube and 17 curved quadrilateral thick shell elements for the Mae West. The elements in the tube have 27 integration points per element and the Mae West elements have 20, 4 per layer with 5 layers through the thickness. It is through these integration points that the temperatures are loaded onto the structural model. Since the thermal data was supplied at only 5 axial locations and was needed throughout the entire model, it was necessary to interpolate the temperatures at the integration points from the known thermal data (see Appendix A).

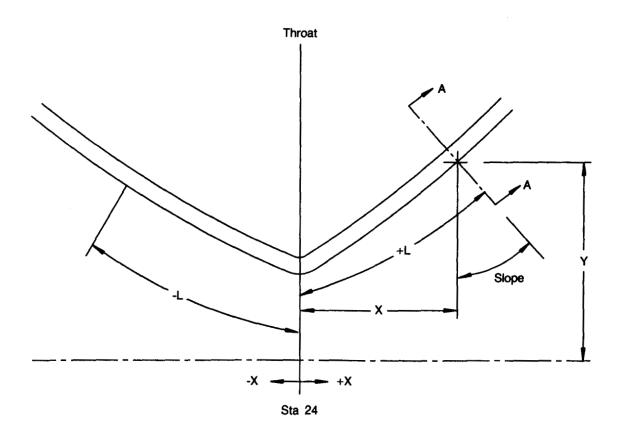
The temperatures in the Mae West were assumed to be the same as the temperatures in the top side of the tube, the side near the Mae West, and constant through the thickness. MARC has the provisions to allow the user to write subroutines to tailor the deck to a particular job. This proved to be a great asset for the purpose of loading the temperatures. The subroutine NEWSV was written to take the interpolated integration point values and do the following:

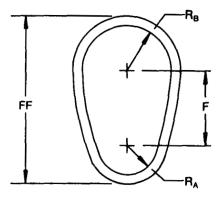
- 1. Convert the temperature from Rankine to Fahrenheit
- 2. Multiply the temperature by the appropriate scale factor
- 3. Take the temperatures from the appropriate integration points of the tube and apply them to the corresponding integration points in the Mae West.

The scale factor was used because transient thermal data was needed but was not available. The heat transfer analysis was a quasi 3-D analysis which did not allow for heat transfer along the length of the tube and was not a transient analysis. By using the scale factor, it was possible to step between the known flight points and make the thermal data appear transient. This is not as good as a 3-D transient thermal analysis but was the best approximation with the available data.

A computer program was written to calculate the nodal coordinates of the tube (Figure 24) using data from Table 4 as input. The Mae West coordinates were calculated by hand. Even though the Mae West is brazed to the tubes, it was decided not to model the silver braze. The reasons being the lack of sufficient material property data, and the feeling that the gain in accuracy would not be worth the added model complexity, and additional computer time and space required.

Because the Mae West and tube were of different element types, a set of tying equations had to be written. These equations define the relationship between the displacements in the Mae West and those in the tube. The equations written were for the nodes along the symmetry plane and tied the nodes in the tube element closest to the Mae West to the nodes in the Mae West, (see Figure 22). This meant there was no tying on the adjacent side. While this arrangement over approximates the stiffness of the silver braze on the symmetry plane, it under approximates the stiffness on the adjacent side. This is not an ideal situation, but it was felt that this is the best approximation of the silver braze considering the material property data available. The three degrees of freedom of the tube node were tied to the three displacement degrees of freedom of the Mae West node. This was done in order to allow one of the rotational degrees of freedom of the Mae West to be restrained.





FDA 329767

Figure 24. Table 4 Data Headers

Because the tubes are arranged around the chamber/primary nozzle in a circular fashion, boundary conditions on the adjacent side must be input in such a way as to allow for radial growth. To accomplish this, the coordinate system of the nodes along the adjacent side of the tube were rotated from the global system to one in which the X direction lies along a radial line from the center line of the throat outward towards the adjacent side of the tube (Figure 25). Then the nodes with the rotated coordinate system were placed on rollers. The nodes along the symmetry plane were placed on rollers in the vertical direction (i.e., the "Y" direction). To restrict rigid body motion, one node on the end of the tube closest to the injector was restrained in a direction corresponding to the engine centerline.

Table 4. Tube Data from Mechanical Design

Sta.			***	a.	Area	No. of Tubes	n.	F. w.	-	Equiv Tube	_
<i>No.</i>	<u> </u>	<u> </u>	FF	Slope	<i>ID</i>	Around	RA	RB	F	Dia	L
1	-14.550	5.1315	0.2026	0.0000	0.0224	180	0.07789	0.07826	0.02097	0.195	-15.044
2	-13.050	5.1174	0.2029	-0.0150	0.0224	180	0.07764	0.07802	0.02174	0.195	-13.544
3	-11.350	5.0966	0.2033	-0.00533	0.0224	180	0.07727	0.07767	0.02287	0.195	-11.844
4	-9.050	5.0603	0.2040	-0.04511	0.0224	180	0.07662	0.07706	0.02485	0.195	-9.543
5	-7.250	4.8989	0.2072	-0.14185	0.0222	180	0.07374	0.07432	0.03366	0.195	-7.735
6	-6.950	4.8535	0.1941	-0.16038	0.0201	180	0.07293	0.07332	0.02236	0.186	-7.432
7	-6.550	4.7845	0.1862	-0.18446	0.0187	180	0.07170	0.07199	0.01697	0.180	-7.026
8	-6.150	4.7060	0.1830	-0.20800	0.0179	180	0.07030	0.07058	0.01667	0.177	-6.618
9	-5.750	4.6173	0.1801	-0.23693	0.0172	180	0.06872	0.06900	0.01692	0.174	-6.209
10	-5.250	4.4875	0.1765	-0.28471	0.0163	180	0.06640	0.06670	0.01791	0.170	-5.692
11	-4.850	4.3643	0.1727	-0.33241	0.0154	180	0.06419	0.06450	0.01854	0.166	-5.273
12	-4.450	4.2204	0.1663	-0.38870	0.0141	180	0.06162	0.06190	0.01725	0.160	-4.848
13	-4.150	4.0968	0.1625	-0.43520	0.0133	180	0.05940	0.05970	0.01791	0.156	-4.524
14	-3.850	3.9596	0.1602	-0.48022	0.0126	180	0.05695	0.05727	0.02052	0.1528	-4.194
15	-3.450	3.7515	0.1546	-0.56688	0.0113	180	0.05322	0.05356	0.02229	0.1465	-3.743
16	-3.050	3.5028	0.1521	-0.65998	0.0103	180	0.04878	0.04920	0.02864	0.1417	-3.272
17	-2.550	3.1883	0.1458	-0.58321	0.0088	180	0.04324	0.04374	0.03331	0.1337	-2.681
18	-1.950	2.8805	0.1319	-0.43896	0.0069	180	0.03783	0.03831	0.03023	0.1209	-2.006
19	-1.450	2.6927	0.1332	-0.31299	0.0065	180	0.03453	0.03516	0.03801	0.1194	-1.472
20	-0.950	2.5648	0.1319	-0.20324	0.0060	180	0.03228	0.03299	0.04116	0.1170	-0.956
21	-0.550	2.5015	0.1332	-0.10796	0.0059	180	0.03117	0.03194	0.04455	0.1170	-0.551
. 22	-0.250	2.4803	0.1336	-0.04543	0.0059	180	0.03080	0.03159	0.04568	0.1170	-0.250
23	-0.150	2.4759	0.1337	-0.03999	0.0059	180	0.03072	0.03152	0.04592	0.1170	-0.150
. 24	0.0000	2.4724	0.1337	0.0000	0.0059	180	0.03066	0.03146	0.04610	0.1170	Throat
25	0.0403	2.4741	0.1348	0.08605	0.0060	180	0.03068	0.03150	0.04714	0.1177	0.040
26	0.0791	2.4791	0.1360	0.17806	0.0061	180	0.03076	0.03159	0.04813	0.1185	0.080
27	0.1185	2.4876	0.1371	0.26068	0.0061	180	0.03090	0.03173	0.04895	0.1193	0.120
28	0.1593	2.5002	0.1381	0.36049	0.0063	180	0.03110	0.03192	0.04958	0.1201	0.163
29	0.1946	2.5146	0.1390	0.45524	0.0063	180	0.03134	0.03213	0.04999	0.1208	0.201
30	0.2619	2.5522	0.1407	0.67173	0.0065	180	0.03194	0.03267	0.05054	0.1223	0.278
31	0.3617	2.6205	0.1429	0.69140	0.0069	180	0.03314	0.03387	0.05038	0.1246	0.399
32	0.5588	2.7593	0.1475	0.71501	0.0077	180	0.03559	0.03630	0.05010	0.1293	0.640
-											
33	0.6851	2.8504	0.1504	0.72648	0.0082	180	0.03720	0.03790	0.04976	0.1323	0.796
34	0.8282	2.9552	0.1536	0.73725	0.0088	180	0.03905	0.03975	0.04931	0.1357	0.973
35	0.9869	3.0730	0.1572	0.74707	0.0095	180	0.04113	0.04182	0.04874	0.1395	1.171
36	1.1605	3.2035	0.1612	0.75575	0.0102	180	0.04344	0.04411	0.04811	0.1437	1.388
37	1.3482	3.3461	0.1654	0.76316	0.0111	180	0.04596	0.04662	0.04731	0.1482	1.623
38	1.5492	3.5001	0.1700	0.76923	0.0121	180	0.04868	0.04933	0.04648	0.1531	1.877
39	1.7628	3.6650	0.1748	0.77391	0.0132	180	0.05160	0.05223	0.04549	0.1583	2.147
40	1.9884	3.8401	0.1799	0.77718	0.0144	180	0.05470	0.05531	0.04443	0.1638	2.432
41	2.2258	4.0247	0.1853	0.77901	0.0157	180	0.05796	0.05856	0.04330	0.1696	2.733
42	2.7339	4.4203	0.1967	0.77876	0.0187	180	0.06496	0.06552	0.04071	0.1819	3.377
43	3.0027	4.6297	0.2028	0.77695	0.0204	180	0.06867	0.06921	0.03945	0.1885	3.718
44	3.2831	4.8467	0.2093	0.77389	0.0222	180	0.07251	0.07304	0.03825	0.1954	4.072
45	3.8721	5.2998	0.2225	0.76505	0.0262	180	0.08054	0.08104	0.03540	0.2096	4.815
46	4.1809	5.5353	0.2297	0.75943	0.0285	180	0.08471	0.08518	0.03427	0.2172	5.204
47	4.5014	5.7765	0.2367	0.75294	0.0308	180	0.08898	0.08944	0.03278	0.2248	5.605
48	4.8260	6.0215	0.2440	0.74620	0.0334	180	0.09332	0.09376	0.03141	0.2326	6.011
49	5.5132	6.5273	0.2597	0.73069	0.0390	180	0.10229	0.10270	0.02924	0.2491	6.865
50	6.2349	7.0487	0.2760	0.71391	0.0453	180	0.11153	0.11192	0.02710	0.2662	7.755

42

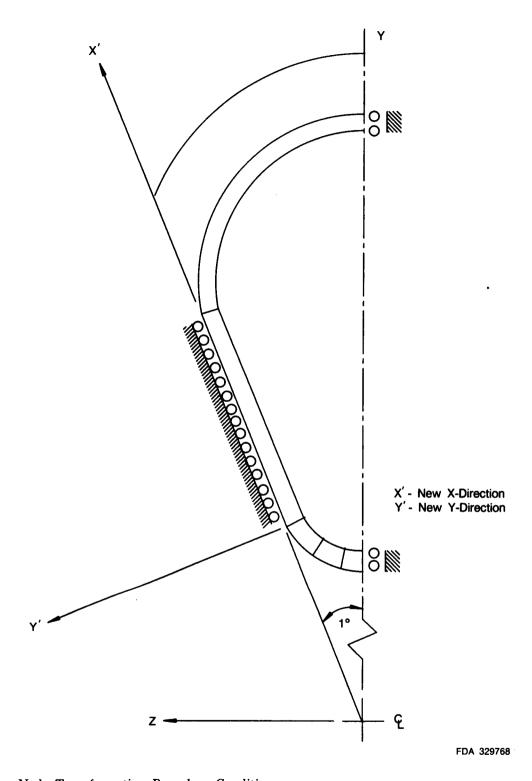


Figure 25. Node Transformation Boundary Conditions

The analysis of the RL10-IIB was actually done twice. The reason for this was the stress strain curve available when the first one was done was for high strength AISI 347 stainless steel. While the tubes are made of AISI 347, they lose some of their strength during the forming and

heat treat processes they go through. In the first analysis, the shape of the stress strain curve was assumed constant with temperature. The stress strain curve was input in a slope breakpoint fashion. With the slope being the change in stress over the change in equivalent plastic strain, and the breakpoint being the equivalent plastic strain at which the corresponding slope becomes effective. Since it was unknown how the stress strain curve changed with temperature this was the only way to input the stress strain data.

When it was decided that analyses of the RL10A-3-3, -3A, and -3B chambers would be done, a request was sent to the P&W Materials Lab to determine material properties and stress strain curves at various temperatures for the actual tube material. The analysis of the RL10-IIB was done again with the material property data provided by the lab. This was done so that there would be as much consistency as possible between all three analyses. The new stress strain curves were input through user defined subroutine WKSLP. In this subroutine the stress strain curve versus temperature is input in equation form. This provides for a good match of the stress strain curve at all temperatures. For additional information see Appendix B.

Other material properties were input as a function of temperature. These were Young's Modulus, proportional limit, instantaneous coefficient of thermal expansion, and Poission's ratio. Input of these was in the slope breakpoint fashion. This time the slope was the change in property per change in temperature, and the breakpoint being the temperature at which the corresponding slope becomes effective. The base values for these properties were input on the property card for the initial stress free temperature, which for this case was $-300^{\circ}F$.

From -300° F the analysis progressed incrementally through the four remaining flight points, tank head idle, pumped idle, full thrust, and shutdown. Table 5 shows the increment at which each of these conditions occurred. In total the analysis ran for 32 increments, 0 to 31. A strain range of 2.44×10^{-2} was calculated, which translates into a life of 230 cycles. This life is based on a 2σ LCF curve (see Appendix B). With failure occurring at approximately 0.5 inch in front of the throat. This 230 cycle life is based upon all of the cycles being full thrust cycles. Cycle life could be increased by knowing the number of tank head idle, pumped idle, and full thrust cycles that comprise a mission. To accurately calculate the strain range for the pumped idle condition only and the tank head idle condition only, the analysis would have to be continued for two more cycles. One cycle starting where this analysis ended, going to tank head idle and back to shutdown. The other would go from shutdown to pumped idle and back to shutdown. An equation for the approximation of partial lives can be found in Appendix C. This equation is based on approximate strain ranges for the partial power cycles, and should not be used to predict partial power lives. It is only to give an indication of the trend taken by including the partial power cycles in the life calculations.

Table 5. Flight Point and Corresponding Increment in the 32 Increment Analysis

Flight Point	Increment
Tank Head Idle	8
Pumped Idle	12
Full Thrust	19
Shutdown	31

RL10A-3-3

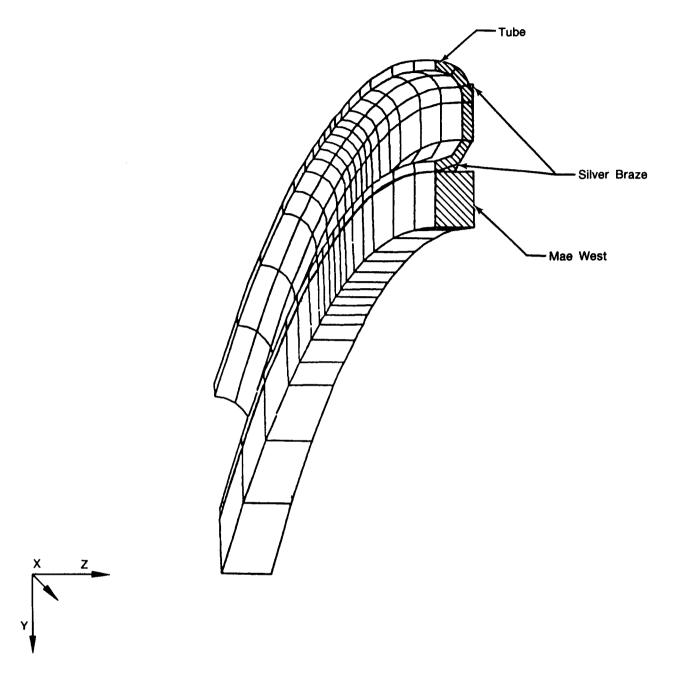
The analysis of the RL10A3-3 was done to compare the results of this analysis with engine test history and to calibrate the analyses done on the RL10-IIB, RL10A-3-3A, and the

RL10A-3-3B. Unlike the Derivative IIB the RL10A-3-3 operates at only one condition, full thrust. This means that the load cycle for this analysis was cryogenic pre-ignition, full thrust, and shutdown. It was the strain range generated by this cycle that was used in the LCF calculations.

Solutions to many of the problems encountered in the analysis of the Derivative IIB were implemented in this analysis. The new material properties used in second RL10-IIB analysis were used here as well. The RL10-IIB thermal data provided was for only five axial locations, did not allow for heat transfer along the length of the tube, and was not a transient analysis. Because this problem is almost totally thermally driven, it was felt that more detailed thermal data was required. So, even though a heat transfer analysis had been completed, similar to the one done for the RL10-IIB, it was decided to do a MARC heat transfer analysis. MARC was chosen because it allows the use of a common stress-heat transfer model. This means that there is a one-to-one correspondence between where the temperatures are output in the heat transfer analysis and where they are required for input in the stress analysis. The heat transfer model did require the addition of a few elements to model the silver braze. These elements were left out of the stress model because of a lack of good material property data for the silver braze, as well as the feeling that the accuracy gained by modeling them would not be worth the additional CPU time and space required if they were included. Figures 26 and 27 show the heat transfer and stress models respectively.

The hotspot in the chamber/nozzle was identified by a 2-D heat transfer analysis, and was located 1.67 inches in front of the throat. Again it was decided to construct a model spanning from one inch in front of the hotspot to one inch behind the hotspot. The nodal coordinates were calculated by the same computer program used to calculate the coordinates of the RL10-IIB. Some small modifications had to be made to the input to allow for the different geometry of the RL10A-3-3. The data for input was supplied by the mechanical design and can be found in Table 6. Again the large thermal gradients dictated a finer breakup on the bottom of the tube and in the area of the hot spot. Even though the models of the RL10-IIB and the RL10A-3-3 have the same number of elements, 102, there is an important difference. In the RL10-IIB the 85 elements comprising the tube are 20-node brick elements and the 17 elements in the Mae West are thickshell elements. For the RL10A-3-3 however, all 102 elements are 20-node bricks. This was done to allow for the necessary input to the Mae West in the thermal analysis. The use of only 20-node brick elements turned out to be an advantage in the stress analysis. The thick-shell elements used in the previous analysis had 5 degrees of freedom per node where the brick elements have only 3 degrees of freedom per node. Also, it was not necessary to tie the tube elements to the Mae West elements since they were of the same element type and shared coincident nodes along a common edge. The reduction in the number of degrees of freedom per node and the fact that no tying was required between the Mae West and the tube elements resulted in a reduction of more than one half in the amount of computer time and space required to do the analysis.

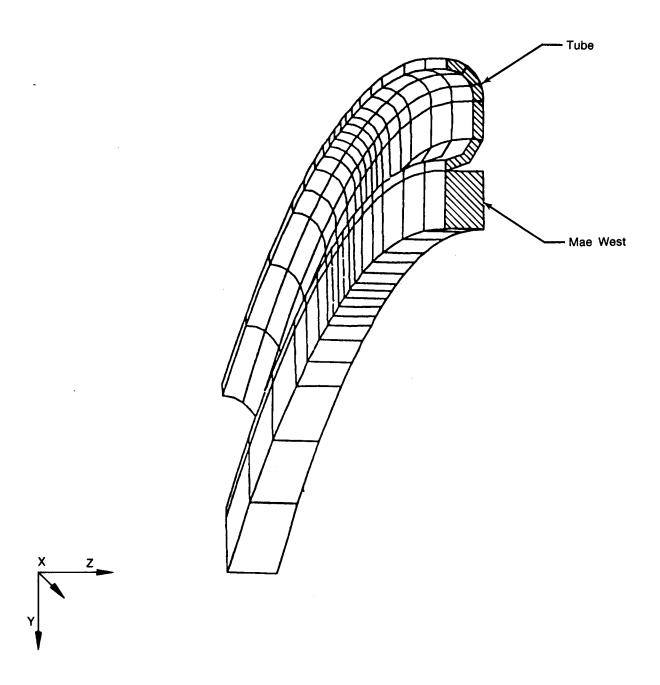
With the new thermal analysis, the input temperatures were stored on a tape. To load these temperatures subroutine NEWSV was still used but had to be rewritten to access the temperatures from the tape. Another subroutine, PLDUMP, was incorporated into the NEWSV subroutine to read the temperatures from the tape into memory. Then NEWSV read the temperatures from memory, converted them from Rankine to Fahrenheit, and applied them to the integration points. No scaling or interpolation of temperatures was needed as in the previous analysis because the MARC heat transfer analysis was a 3-D transient analysis.



FD 329769

Figure 26. RL10A-3-3 Transient MARC Heat Transfer Model

As in the analysis of the RL10-IIB, it was necessary to allow for radial growth when inputting the boundary conditions. This was accomplished in the same fashion as before: by rotating the coordinate system of some of the nodes along the adjacent side of the tube (Figure 25). This allowed them to be placed on rollers in the proper plane so as to allow for radial growth. The nodes along the symmetry side were placed on rollers in the vertical direction. To restrict rigid body motion, a node at the end of the tube nearest the throat was restrained in a direction along the length of the tube.



FD 329770

Figure 27. RL10A-3-3 Stress Model

Input of material properties was as in the previous analysis. Subroutine WKSLP was used to input the stress strain curve versus temperature, and the other material properties were defined in slope breakpoint fashion in the input data set.

Table 6. Tube Data from Mechanical Design (Ref. Figure 24)

Y	Slope	RA	RB	F	Number of Tubes Around
3.5600	-0.58375	0.049830	0.050519	0.045701	180
3.2190	-0.38976	0.043856	0.044686	0.051043	180
2.9750	-0.38976	0.039527	0.040377	0.052212	180
2.7940	-0.38976	0.036316	0.037145	0.050933	180
2.6680	-0.18921	0.034124	0.034967	0.049147	180
2.5940	-0.10699	0.032819	0.033613	0.045723	180

The analysis was incremental, with increment 0 being the first increment, increment 31 being the last, and the full thrust condition occurring at increment 14. A life of more than 290 cycles was predicted from a strain range of 2.140×10^{-2} with failure occurring at 1.8 inches in front of the throat. This cycle life is the number of cycles to crack and was obtained from a 2σ strain range versus cycles-to-crack curve for AISI 347 in a hydrogen atmosphere at 1400°F (see Appendix B). The test stand experience shows that the chamber with the greatest numbers of cycles to date has 161 and the most time accumulated on a chamber is eight hours.

This analysis was accomplished more efficiently than the analysis of the Derivative IIB. There were several reasons for this:

- 1. Most of the computer problems (i.e., how much space was required, writing new subroutines from scratch, etc.) were solved on the first analysis
- 2. The reduction in the amount of CPU time required meant that the job would be in the computer for a shorter period of time which means less chance of the job running when a computer problem occurs
- 3. The program to generate the geometry was already written; only modifications to the input were required
- 4. Since the input temperatures were provided from MARC heat transfer, it was not necessary to calculate the integration point locations, and interpolate the temperatures needed at these locations, from the temperatures known at only a few locations.

RL10A-3-3A

The RL10A-3-3A is similar to the RL10A-3-3 except it has a silver insert in the throat. The load cycle is the same, cryogenic pre-ignition, full thrust, and shutdown. As in the analysis of the RL10A-3-3 it was the strain range produced by this cycle that will be used in the LCF calculation.

A 2-D heat transfer analysis indicated that the hot spot would be 2.167 inches in front of the throat. This is 0.5 inch closer to the injector than in the RL10A-3-3. The shift in the location of the hot spot is caused by the silver insert. Since the shift in the hot spot was only 0.5 inch and the RL10A-3-3 and RL10A-3-3A have the same tube geometry, it was decided to use the stress model from the RL10A-3-3 analysis. This included a distance of 0.5 inch from the anticipated maximum stress location to the upstream end of the span modeled.

It was decided to do a MARC heat transfer analysis for the RL10A-3-3A, for the same reasons one was done on the RL10A-3-3. Transient 3-D thermal data was needed at locations corresponding to the input in the stress analysis. The RL10A-3-3 heat transfer model had to be modified to include the silver insert. The silver braze extended only slightly into the region modeled so only a few elements had to be added to the end of the heat transfer model. Figure 28 shows the heat transfer model for the RL10A-3-3A.

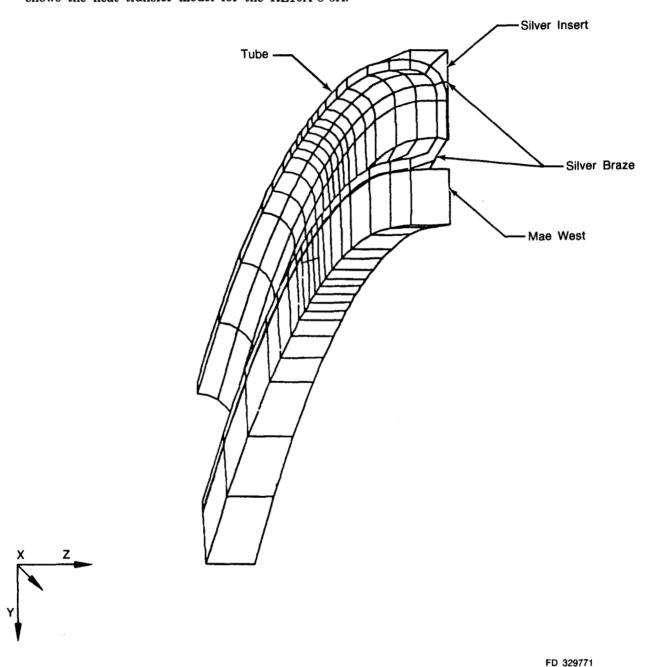


Figure 28. RL10A-3-3A Heat Transfer Model With Braze in Throat

Having the temperatures supplied on tape as with the RL10A-3-3 allowed use of subroutines NEWSV and PLDUMP without modification. The same is true of subroutine

WKSLP and the rest of the material properties. The pressure input had to be changed to match the pressure profile of the RL10A-3-3A, and the increments used from the thermal tape had to be changed, to provide a good thermal profile.

A life of more than 297 cycles was predicted based on a strain range of 2.101×10^{-2} . As with both previous analyses, the cycle life is cycles to crack, and, as with the analysis of the RL10A-3-3, is based on a 2 σ curve for AISI 347 in a hydrogen atmosphere at 1400°F (see Appendix B).

RL10A-3-3B

The RL10A-3-3B is similar to the RL10A-3-3A except for an increase in mixture ratio from 5.0 to 6.0, and reduction of thrust from 16,500 to 15,000 pounds. The maximum temperature in the throat is 1705°F. As with the RL10A-3-3A there is only one operation condition, full thrust. The strain range produced by the shutdown to full thrust to shutdown cycle is used in the LCF calculations.

Again a 2-D heat transfer analysis was used to indicate a hotspot location, 2.167 inches in front of the throat. As with the RL10A-3-3A this is 0.5 inch closer to the injector and it was decided to use the same stress model that was used in the RL10A-3-3A analyses. Because the same model was being used, the subroutines (NEWSV, PLDUMP, WKSLP) could be used, as well as the same material properties.

A MARC heat transfer analysis was done to supply the temperatures. The reasons for this are the same as in the previous analyses. The heat transfer analysis had to be redone because of the change in the mixture ratio.

A strain range of 2.25×10^{-2} was calculated giving a life of more than 275 cycles. This number is cycles to crack and is based on a 2σ curve for AISI 347 at 1400°F in a hydrogen atmosphere (see Appendix B).

REFERENCES

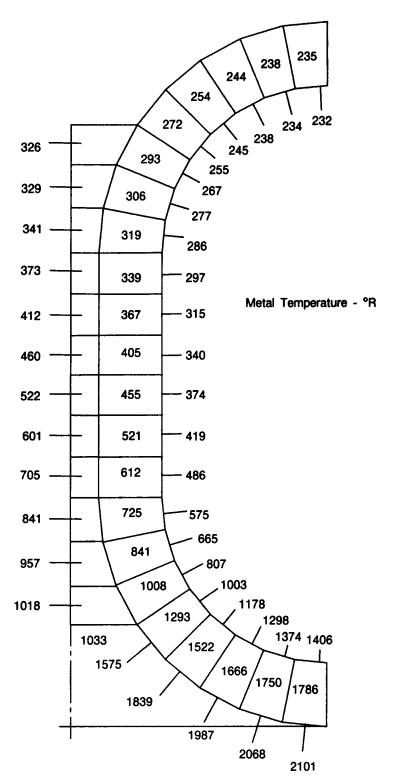
NASA Report CR135022, Carl E. Jaske, Richard C. Rice, Richard D. Bucheit, Donald B. Roach, and Theodore L. Porfilio, "Low Cycle Fatigue of Type 347 Stainless Steel and Hastealloy Alloy X in Hydrogen Gas and in Air at Elevated Temperatures."

APPENDIX A
THERMAL MODEL NODES AND STRESS MODEL INTEGRATION POINTS

Thermal model nodes and stress model integration points were reconciled as follows:

- At the five stations where temperatures are known, surface temperatures were assigned to the closest integration point and element temperatures were assigned to interior integration points, averaging where necessary (see Figures 29, 30, and 31).
- The temperatures at all of the remaining integration points were interpolated from the values at the five defining stations. Coordinates of the integration points were calculated by a Speakeasy program.

PRECEDING PAGE BLANK NOT FILMED



FDA 329776

Figure 29. RL10 Derivative II — Sample Heat Transfer Data

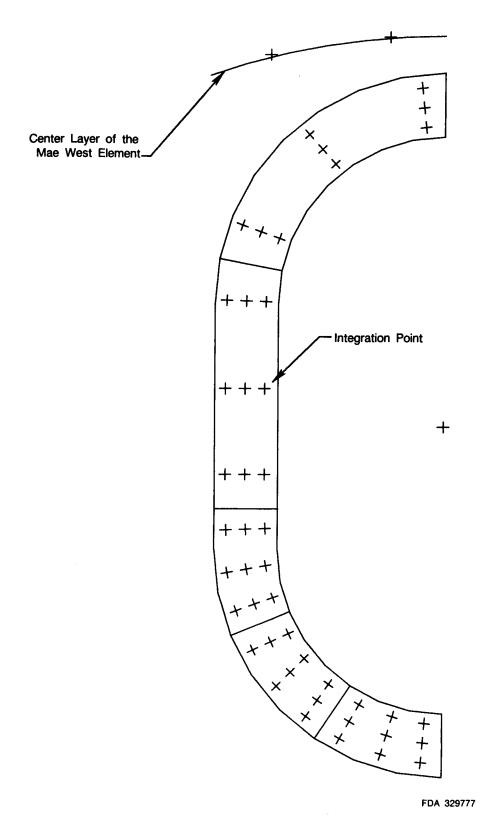


Figure 30. RL10 Derivative II — Slice of the Model at a Plane Containing Integration Points

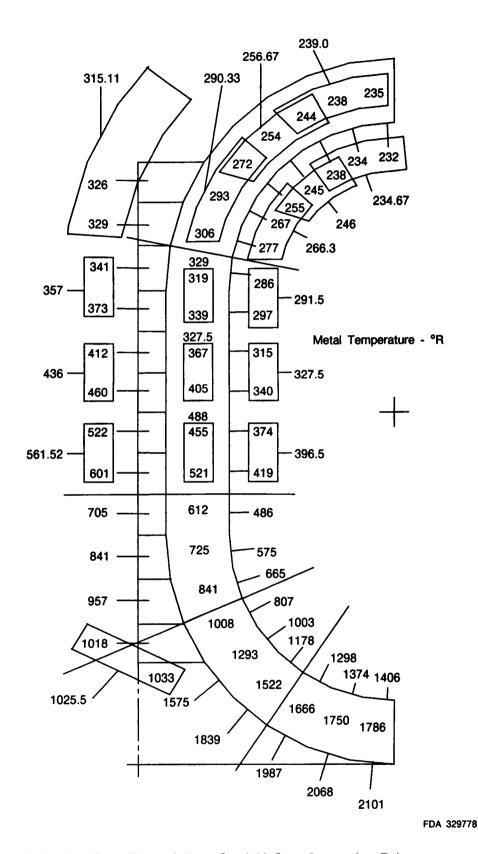


Figure 31. RL10 Derivative II - Thermal Data Overlaid Onto Integration Points

APPENDIX B PROPERTIES OF MATERIALS USED IN ANALYSES OF FOUR CHAMBERS

A. INTRODUCTION

The material properties used in the analyses of all four chambers were supplied by the Pratt & Whitney Materials Engineering and Technology Laboratory and can be found in paragraph B below. MARC subroutine WKSLP was used to input the stress-strain curve versus temperature. MARC supplied the subroutine with temperature and plastic strain, and WKSLP returned a stress value to MARC. The equation used to generate this stress was as follows:

• ss = $ck \times (plastic strain)^{cn}$.

The equation for the ck and cn parameters versus temperature were generated by a regression on the lab data and are as follows:

- $ck = 83855 127.98T + 0.14423T^2 5.3744E-5 \times T^3$
- cn = $0.12037 3.1765E-5 \times T + 6.612E-8 \times T^2 3.3456E-11 \times T^3$

The LCF curves used in these analyses were generated from data in the Reference 1 NASA report (see Attachment 1). Four curves were generated:

- 1. 1600°F in air
- 2. 1600°F in a hydrogen atmosphere
- 3. 1400°F in a hydrogen atmosphere
- 4. 1000°F in a hydrogen atmosphere.

The temperatures shown approximate the predicted temperatures for the three engine operating points.

Using the data in the NASA report as typical, a computer program was written to calculate LCF curves at each temperature. For the 1600°F in air curve, three curves were calculated. There was not enough 1600°F in air data in the report to generate a good confidence level in a curve had one been generated. So, for the 1600°F in air curve, the 1400°F in air data was used as typical for 1400°F; two standard deviations away from that curve was a 1400°F minimum curve, and two standard deviations away from the minimum curve was assumed the 1600°F in air minimum curve. This data and a Weibull analysis using the ratio of the actual to predicted values for the 1400°F air data were plotted to check the validity of these assumptions.

At the engine operating mixture ratio, the exhaust is hydrogen rich. Because of this, a new curve for 1600°F was generated using the data for 1600°F in a hydrogen atmosphere. Two curves were generated, one for 1600°F typical data and the other two standard deviations away to be the minimum curve. A Weibull was again plotted to verify the curves. At other temperatures of interest, 1400°F and 1000°F, curves were again generated and Weibulls plotted. Tables 7, 8, 9, and 10 contain the input data for the Speakeasy program for 1600°F air, 1600°F hydrogen, 1400°F hydrogen, and 1000°F hydrogen, and 35 are the LCF curves for 1600°F air, 1600°F hydrogen, 1400°F hydrogen, and 1000°F hydrogen respectively. All lives are based on the 2 σ LCF curves with a 50 percent confidence band. Copies of the Weibulls are included in this appendix.

Table 7. 1400°F, Air Data

Total Axial Strain Range, %	Fatigue Life, Cycles
4.92	81
5.10	60
5.11	80
3.32	120
2.64	137
3.09	125
2.59	148
3.31	140
3.09	130
1.63	280
1.64	300
1.64	400
1.57	430

Data from NASA Report CR 135022 "Low Cycle Fatigue of Type 347 Stainless Steel and Hastealloy X in Hydrogen Gas and in Air at Elevated Temperatures."

Table B.1, p. 91

77400

Table 8. 1600°F, Hydrogen Data

Total Axial Strain Range, %	Fatigue Life, Cycles
4.96	90
4.93	82
5.32	80
4.97	120
5.30	210
4.97	100
4.96	150
4.95	220
3.20	255
2.96	250
2.97	320
2.98	450
1.70	500
1.50	800
1.47	850
1.48	900
1.44	1000
1.28	1750
1.50	800
1.48	1200
1.44	2100
1.48	1400

Data from NASA Report CR 135022 "Low Cycle Fatigue of Type 347 Stainless Steel and Hastealloy X in Hydrogen Gas and in Air at Elevated Temperatures".

Table 2B, p. 97

1740C

Table 9. 1400°F, Hydrogen Data

Total Axial Strain Range, %	Fatigue Life, Cycles
4.92	104
4.89	103
4.88	111
4.87	128
4.88	123
4.87	150
4.89	160
4.85	182
2.96	185
2.95	222
2.94	217
2.95	243
2.96	200
2.94	235
2.95	270
2.95 2.95	325
2.95 1.49	620
1.49	682
1.45	616
1.49	515
1.50	735
1.46	760
1.49	750
1.50	850

Data from NASA Report CR 135022 "Low Cycle Fatigue of Type 347 Stainless Steel and Hastealloy X in Hydrogen Gas and in Air at Elevated Temperatures".

Table 3B, p. 95

Table 10. 1000°F, Hydrogen Data

Total Axial Strain Range, %	Fatigue Life, Cycles
4.94	120
4.92	121
4.94	141
4.92	147
4.93	153
4.93	156
4.97	166
4.89	165
4.92	171
2.92	288
2.91	307
2.95	331
2.92	336
2.91	361
2.92	367
2.96	385
2.89	382
1.50	1303
1.48	1555
1.49	1812
1.38	1840
1.49	1810
1.48	1949
1.46	2238
1.47	2425
1.39	2495

Data from NASA Report CR 135022 "Low Cycle Fatigue of Type 347 Stainless Steel and Hastealloy X in Hydrogen Gas and in Air at Elevated Temperatures". Table 4B, p. 93

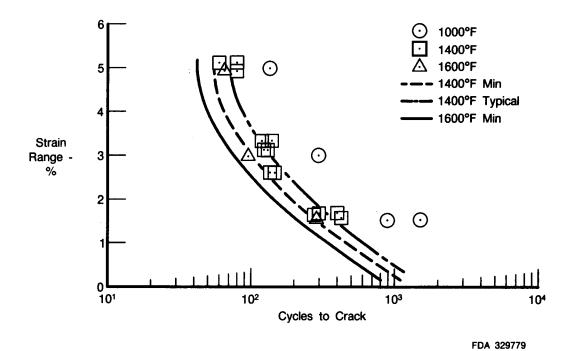


Figure 32. AISI 347 LCF Curves in Air

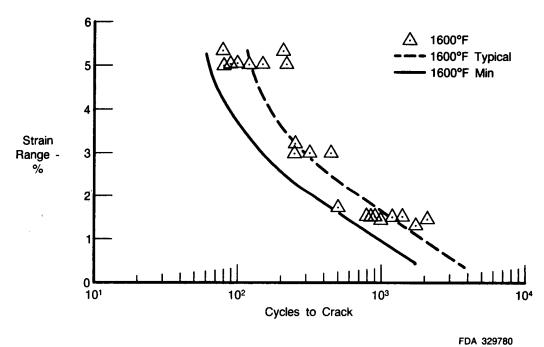


Figure 33. AISI 347 LCF Curves in Hydrogen Atmosphere — 1600°F

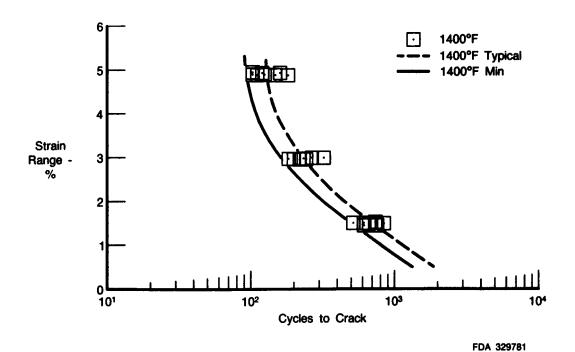


Figure 34. AISI 347 LCF Curves in Hydrogen Atmosphere — 1400°F

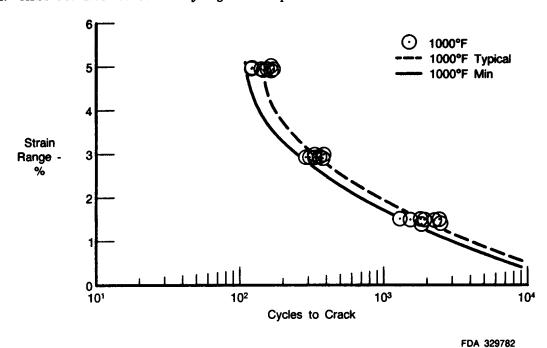


Figure 35. AISI 347 LCF Curves in Hydrogen Atmosphere — 1000°F

B. MATERIALS TEST REPORT

Subject: Tensile Characterization of PWA 770 (AISI 347 Stainless

Steel Tube)

Manufacturing Source: LeFiell Mfg Corporation

Material Source: Superior Tube

Mat'l Configuration: Tube, 0.332 in. O.D., 0.0115-0.0140 in. wall thickness

Part Number: 2099098 SF

The tensile properties of PWA 770 (AISI 347 stainless steel tube) were established in support of design efforts for the RL10 chamber/primary nozzle tubing. This program established the tensile strength (proportional limit, 0.2 percent offset yield, and ultimate), ductility (percent elongation), stress-strain parameters, and the elastic modulus for the tubing at 75, 1000, 1200, 1400, and 1600°F. All curves presented represent the average of two or three tests conducted at each temperature.

Tensile strength and ductility vs temperature curves are presented in Figures 36 and 37, respectively. All test data are listed in Table 11.

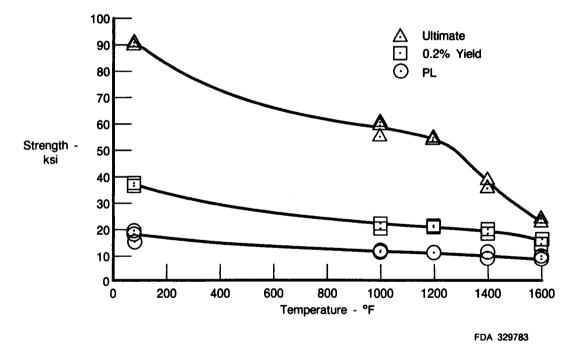


Figure 36. AISI 347 Tensile Strength vs Temperature

Stress-strain parameters are presented graphically in Figures 38 and 39 and are listed in Table 12.

The elastic modulus (static) is presented as a function of test temperature in Figure 40.

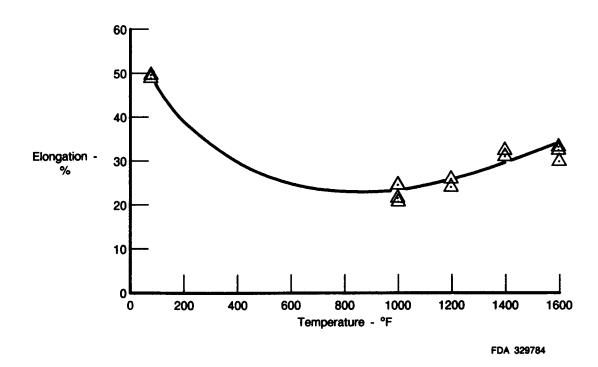


Figure 37. AISI 347 Tensile Ductility vs Temperature

Table 11. Tensile Data for PWA 770 (AISI 347 Stainless Steel Tube)

	Test	3	Strengti	h	Ductility	Elastic
Specimen	Temp	P.L.	0.2% Y	Ult.	El.	Modulus
No.	(°F)	(ksi)	(ksi)	(ksi)	(%)	$(psi \times 10^6)$
1	75	19.2	36.1	89.9	49.0	28.3
2	75	15.1	36.1	89.8	49.0	27.0
3	75	17.9	37.8	90.8	50.0	26.3
4	1000	11.9	22.4	56.6	22.5	19.9
5	1000	11.1	20.0	59.9	25.0	20.2
6	1000	12.6	21.4	60.2	21.0	20.9
7	1200	11.5	20.7	55.3	24.0	19.1
8	1200	11.6	21.9	54.3	26.5	17.9
9	1400	8.5	17.7	35.2	33.0	17.1
13	1400	11.1	20.6	37.9	37.9	17.0
10	1600	8.6	15.1	22.1	32.0	14.3
11	1600	9.3	15.8	22.1	22.1	14.3
12	1600	8.5	15.4	21.8	29.0	14.2

66

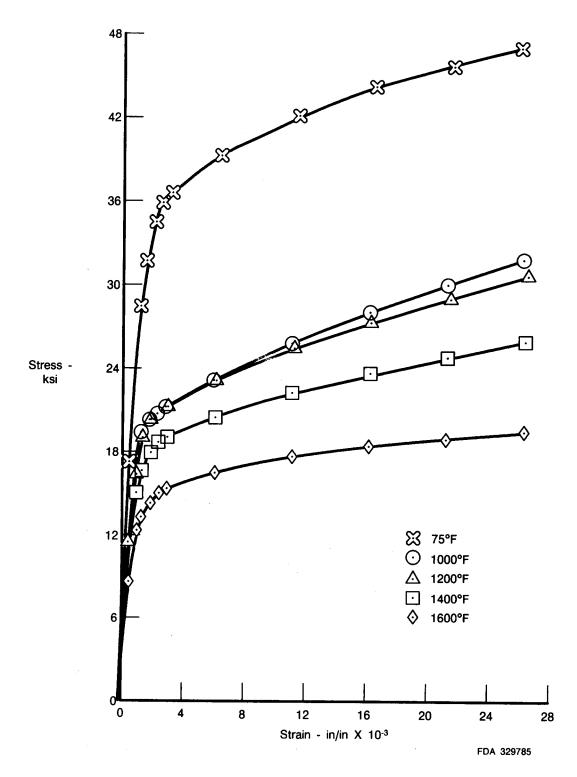


Figure 38. AISI 347 Tensile Stress vs Strain

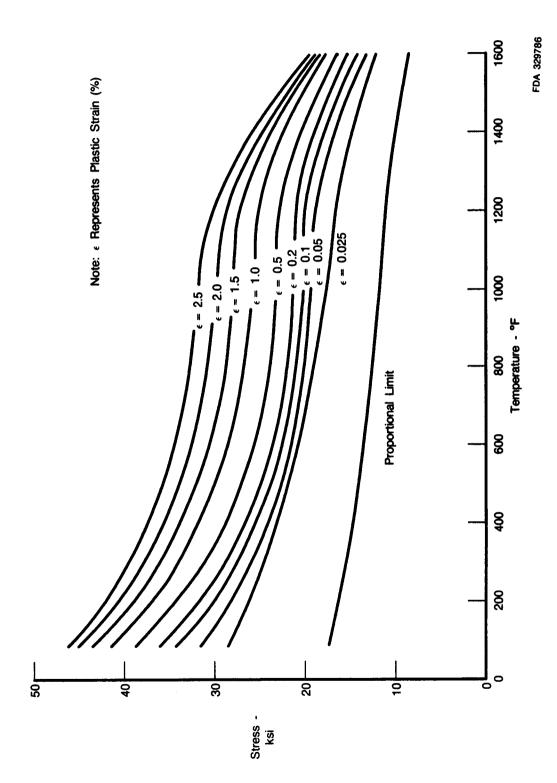


Figure 39. AISI 347 Tensile Stress vs Temperature and Plastic Strain

Table 12. Tensile Stress-Strain Parameters for PWA 770 (AISI 347 Steel Tube)

Plastic Strain	Stress	Elastic Strain	Stress	Elastic Strain	Stress	Elastic Strain
(%)	(ksi)	$in./in. \times 10^{-3}$	(ksi)	$in./in. \times 10^{-3}$	(ksi)	in./in. × 10 ⁻³
(/ 0 /		N 1 (75°F)		N 2 (75°F)	/	N 3 (75°F)
0.0		-	•			•
0.0	19.3	0.68	15.1	0.56	17.9	0.68
0.025	28.9	1.28	27.0	1.24	29.8	1.36
0.050	31.3	1.64	31.2	1.64	33.0	1.72
0.100	34.0	2.24	34.1	2.24	35.6	2.28
0.150	35.4	2.80	35.4	2.40	36.9	2.84
0.200	36.1	3.32	36.1	3.28	37.8	3.36
0.500	38.9	6.40	38.5	6.40	40.6	6.48
1.000	41.6	11.52	41.1	11.48	43.4	11.56
1.500	43.7	16.56	43.0	16.56	45.5	16.64
2.000	45.4	21.64	44.1	21.56	47.2	21.68
2.500	46.8	24.68	45.0	26.60	48.6	26.76
	S/N	4 (1000°F)	S/N	5 (1000°F)	S/N	6 (1000°F)
0.0	11.9	0.60	11.2	0.55	12.6	0.60
0.025	18.7	1.20	17.2	1.05	17.4	1.05
0.050	20.7	1.55	18.€	1.35	19.1	1.35
0.100	21.6	2.10	19.3	1.90	20.3	1.90
0.150	22.0	2.60	19.6	2.40	20.9	2.40
0.200	22.4	3.10	20.1	2.95	21.4	2.95
0.500	24.0	6.15	22.1	6.05	23.6	6.05
1.000	26.5	11.30	24.8	11.15	26.4	11.15
1.500	28.4	16.40	27.1	16.30	28.7	16.25
2.000	30.2	21.45	29.1	21.35	30.7	21.35
2.500	31.9	26.60	31.0	26.45	32.7	26.40
	S/N	7 (1200°F)	S/N	8 (1200°F)		
0.0	11.5	0.60	11.6	0.65		
0.025	16.6	1.05	16.3	1.20		
0.050	18.9	1.40	19.3	1.65		
0.100	20.0	1.90	20.9	2.20		
0.150	20.3	2.50	20.5	2.75		
0.200	20.7	3.00				
0.500	20.7 22.6	6.10	21.9 23.8	3.30 6.40		
1.000	24.7	11.20	23.8 26.2	11.50		
1.500	26.2	16.25	28.4	16.60		
2.000	27.8	21.35	30.2	21.75		
2.500	29.4	26.40	31.9	26.85		
		9 (1400°F)		13 (1400°F)		
0.0	8.5					
0.025	6.5 13.9	0.50	11.1	0.65		
0.050	15.4	1.05 1.40	16.4	1.15		
0.100	16.4 16.6		18.1	1.55		
0.150	17.3	2.00	19.5	2.10		
0.130	17.3 17.7	2.50	20.2	2.60		
0.200		3.05	20.6	3.15		
	19.1	6.10	22.0	6.25		
1.000	20.8	11.20	23.8	11.30		
1.500	21.9	16.30	25.5	16.40		
2.000 2.500	$22.8 \\ 23.6$	21.30 26.35	26.9	21.50		
	7.3 h	2h 3h	28.2	26.60		

Table 12. Tensile Stress-Strain Parameters for PWA 770 (AISI 347 Steel Tube) (Continued)

Strain (%)	Stress (ksi)	Elastic Strain in./in. × 10 ⁻³	Stress (ksi)	Elastic Strain in./in. × 10 ⁻³	Stress (ksi)	Elastic Strain in./in. × 10 ⁻³
	S/N	10 (1600°F)	S/N	11 (1600°F)	S/N	12 (1600°F)
0.0	8.6	0.60	9.3	0.65	8.5	0.60
0.025	12.4	1.15	12.9	1.20	12.2	1.15
0.050	13.2	1.45	13.9	1.50	13.2	1.45
0.100	14.2	2.05	14.9	2.05	14.3	2.05
0.150	14.7	2.55	15.5	2.65	15.1	2.60
0.200	15.1	3.10	15.8	3.15	15.4	3.10
0.500	16.3	6.15	17.0	6.20	16.5	6.20
1.000	17.6	11.25	18.0	11.30	17.7	11.25
1.500	18.4	16.25	18.7	16.30	18.2	16.30
2.000	19.0	21.30	19.2	21.35	18.8	21.35
2.500	19.4	26.35	19.9	26.40	19.1	26.40

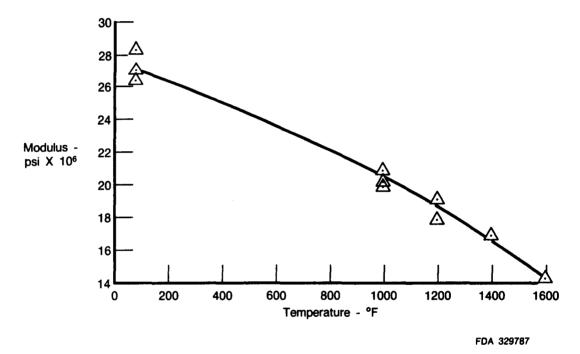


Figure 40. AISI 347 Elastic Modulus vs Temperature

APPENDIX C
STRAIN RANGE VALUES AT PUMPED IDLE AND TANK HEAD
IDLE CONDITIONS

The strain range values for the pumped idle and tank head idle conditions shown in Table 13 are approximate strain ranges. They assume the minimum strain is zero and that the maximum strain occurs at the same location as in the full thrust condition.

Table 13. Approximate Strain Ranges at Three Engine Conditions

Flight Point	Strain Range	Cycles to Crack
Full Thrust	2.44×10^{-2}	230
Pumped Idle	1.20×10^{-2}	620
Tank Head Idle	9.103×10^{-3}	3500
Npi = Number o Nthi = Number	/620) + (Nthi/3500 f Pumped Idle Cyc of Tank Head Idle f Full Thrust Cycle	eles Cycles
		162

To accurately calculate the strain range for the pumped idle and tank head idle conditions the analysis would have be run for two more cycles. One cycle starting from the end of the last analysis, going to tank head idle and back to shutdown; while the other would go to pumped idle and then back to shutdown. Then the maximum strain range for each cycle could be calculated.

Also, since the maximum temperatures at tank head idle and pumped idle are below 1000°F (500°F to 700°F range) LCF curves at temperatures below 1000°F would probably increase the "Cycles to Crack" numbers. Unfortunately the data available in Attachment 1 does not have data for less than 1000°F.

The strain range values are from the RL10-IIB runs with subroutine WKSLP. The "Cycles to Crack" number for full thrust is from the AISI 347 hydrogen atmosphere at 1600°F life curve. The "Cycles to Crack" numbers for tank head idle and pumped idle are from the AISI 347 hydrogen atmosphere 1000°F life curve.

PRECEDING PAGE BLANK NOT FILMED

ATTACHMENT 2 PHOTOGRAPHIC RECORD OF FABRICATION

PRECEDING PAGE BLANK NOT FILMED

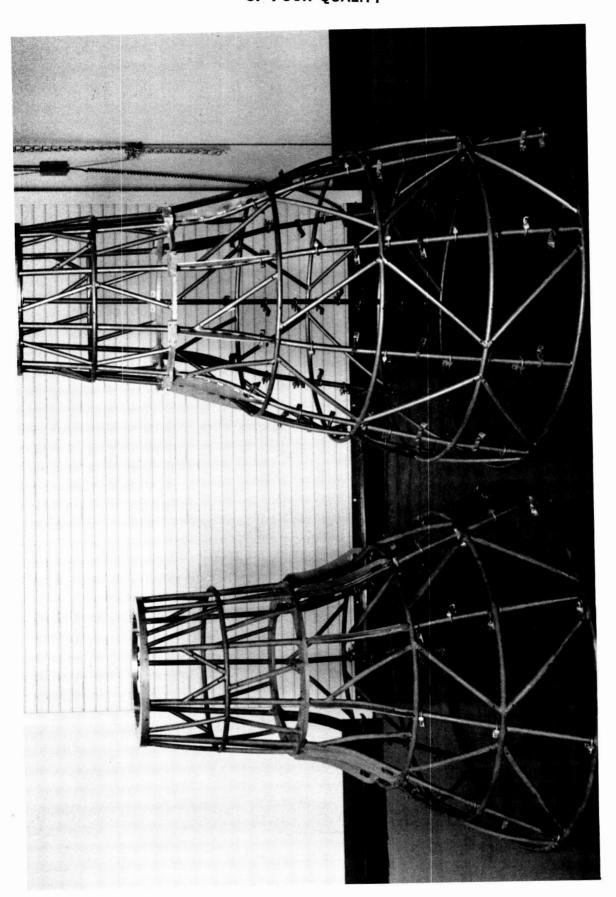


Figure 41. Band Harness — RL10 Derivative II vs RL10A-3-3

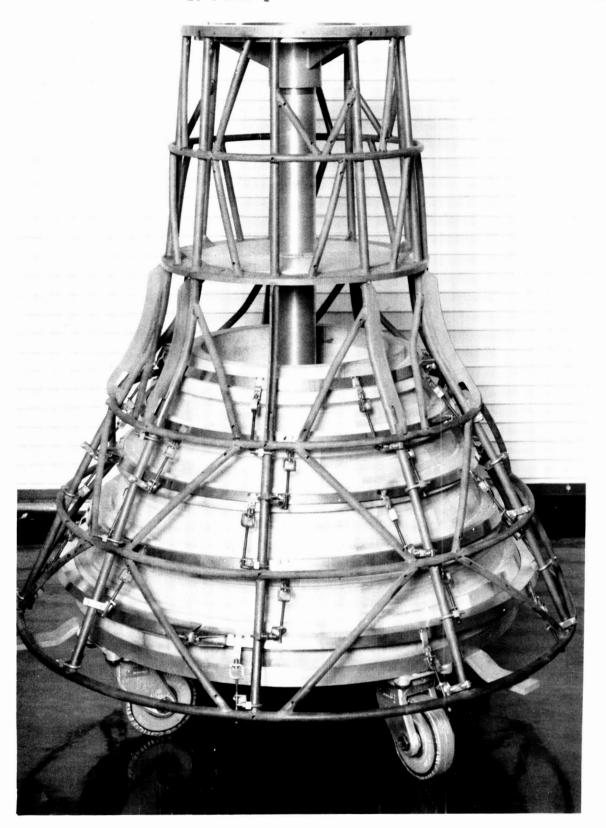


Figure 42. Band Harness With Fixture Bands Installed

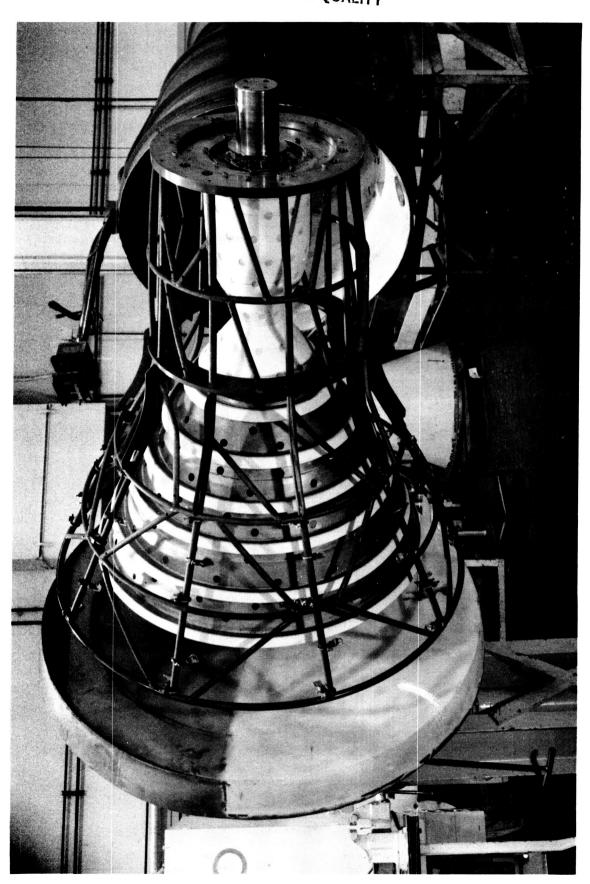


Figure 43. Band Harness and Mandrel Assembled for Curing

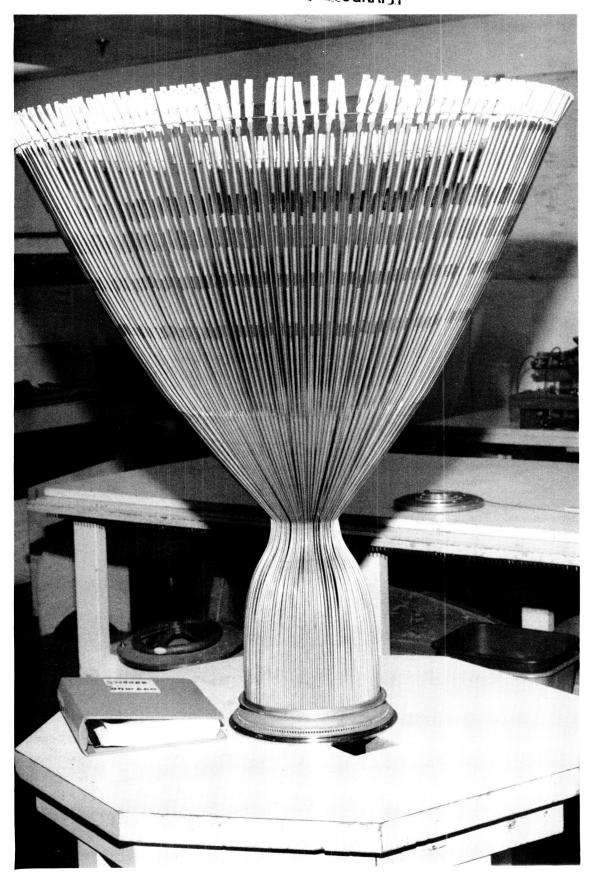


Figure 44. Long Tubes Stacked in Exit Manifold



Figure 45. Hooked Tube Exit Manifold Showing Sockets

ORIGINAL PAGE BLACK AND WHITE PHOTOGRAPH

Figure 46. Long Tube Stack Installed on Mandrel

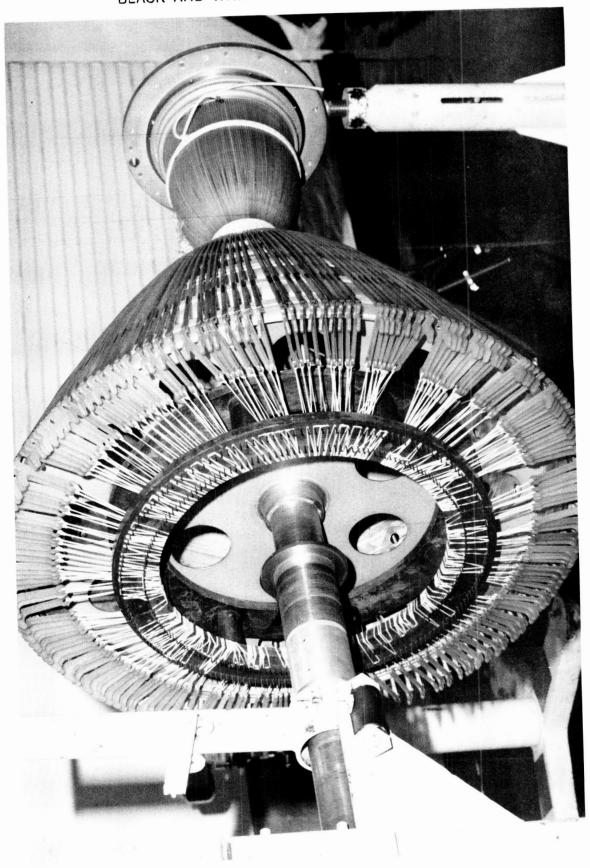
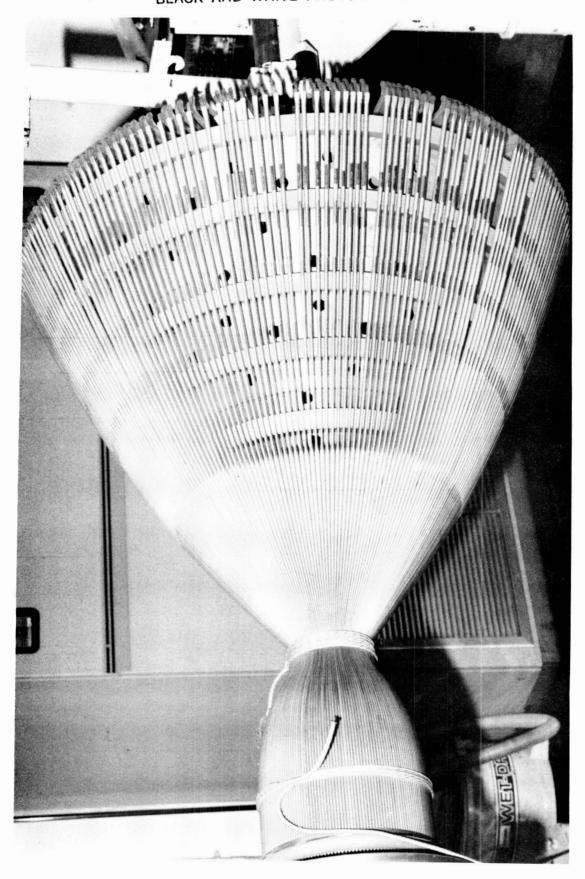




Figure 47. Long Tube Stack on Mandrel With Retaining Hooks

Figure 48. Long Tube Stack Installed on Mandrel



ORIGINAL PAGE IS OF POOR QUALITY

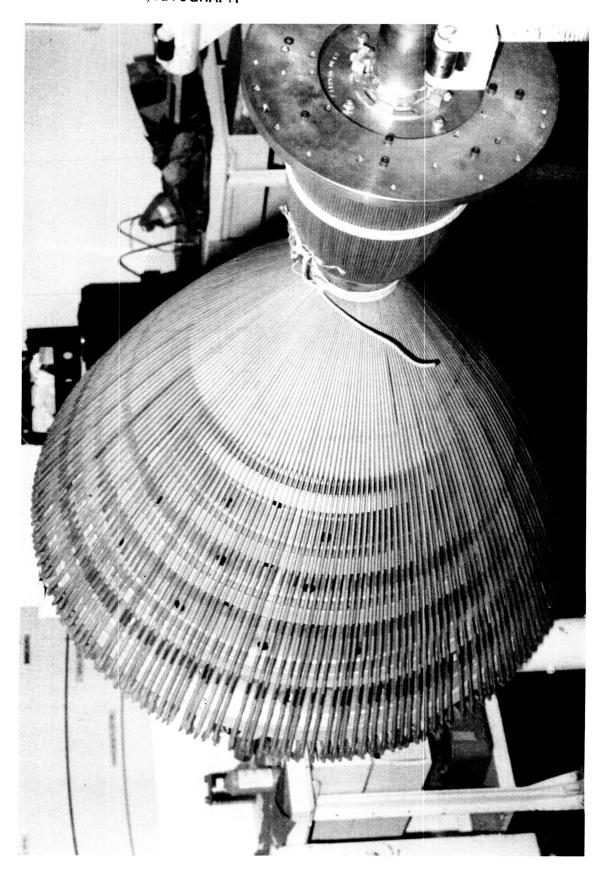


Figure 49. Long Tube Stack Installed on Mandrel



Figure 50. Completed Stack With Short Tubes and Inlet Manifold Installed



Figure 51. Short Tubes and Inlet Manifold Installed

ORIGINAL PAGE BLACK AND WHITE PHOTOGRAPH



ORIGINAL PAGE BLACK AND WHITE PHOTOGRAPH

ORIGINAL PAGE IS OF POOR QUALITY



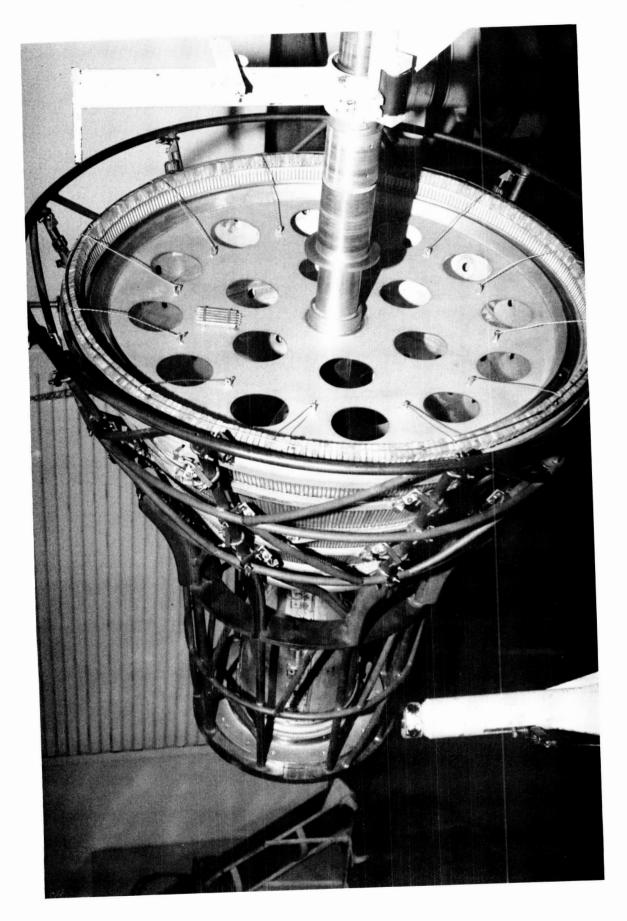
Figure 53. Reinforcing Band Segments Installed With Welded Latches





Figure 55. Band Harness Installation

Figure 56. Completed Assembly Ready for Furnace Braze



ORIGINAL PAGE IS OF POOR QUALITY

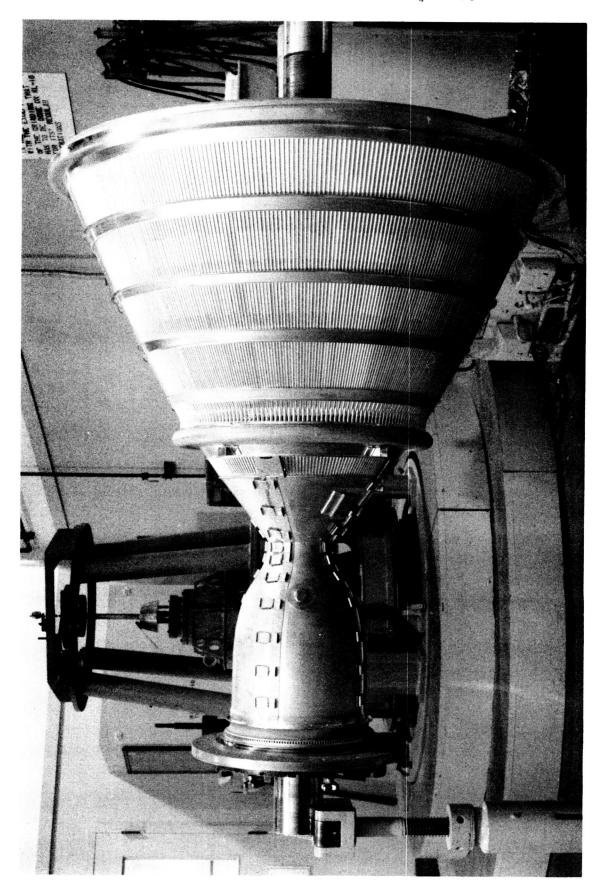
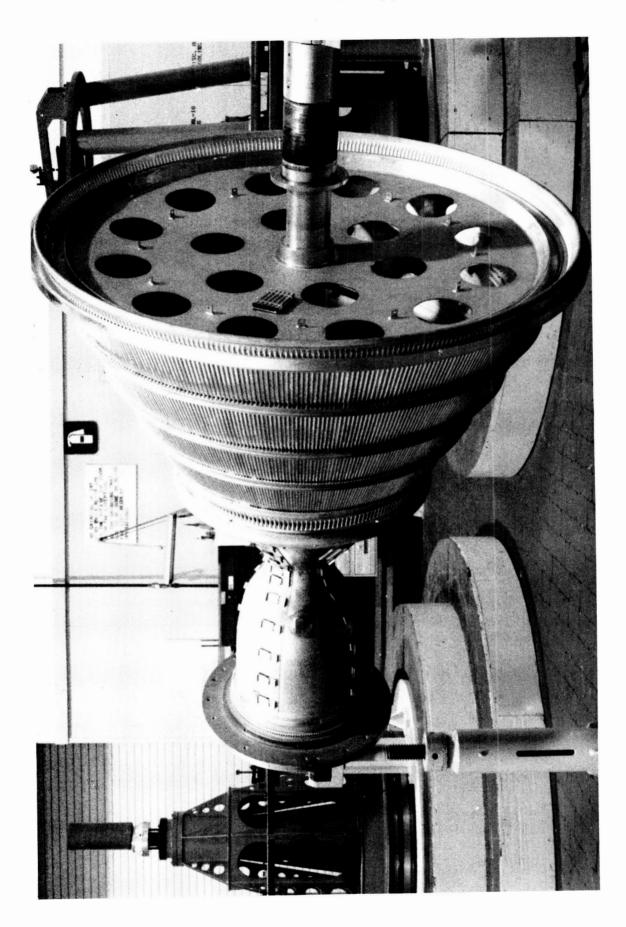


Figure 57. Post-Braze Assembly After Removal From Furnace

Figure 58. Post-Braze Assembly After Removal From Furnace



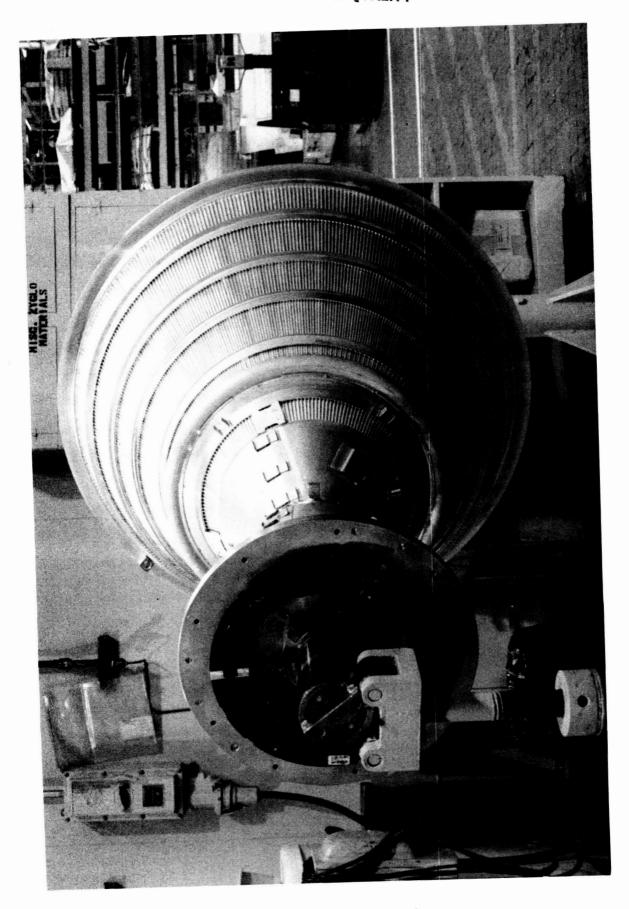


Figure 59. Post-Braze Assembly After Removal From Furnace

ORIGINAL PAGE BLACK AND WHITE PHOTOGRAPH



Figure 60. Brazed Assembly After Removal From Mandrel

Figure 61. Primary Nozzle Interior

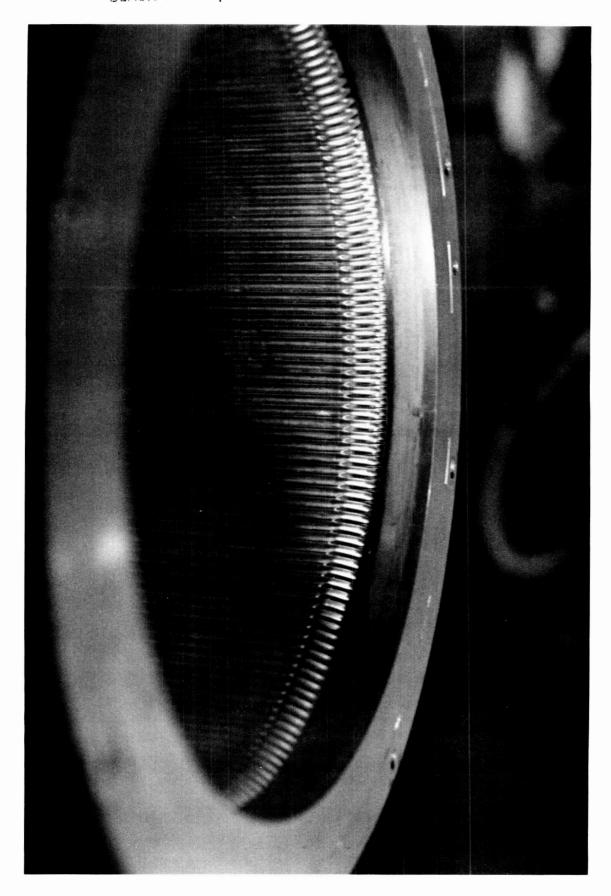


Figure 62. Combustor Chamber Interior Showing Hooked Tubes

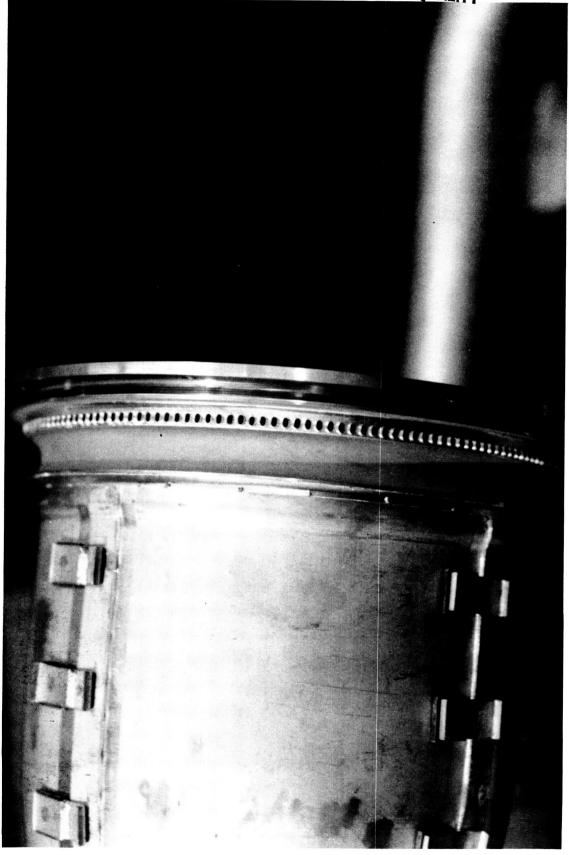
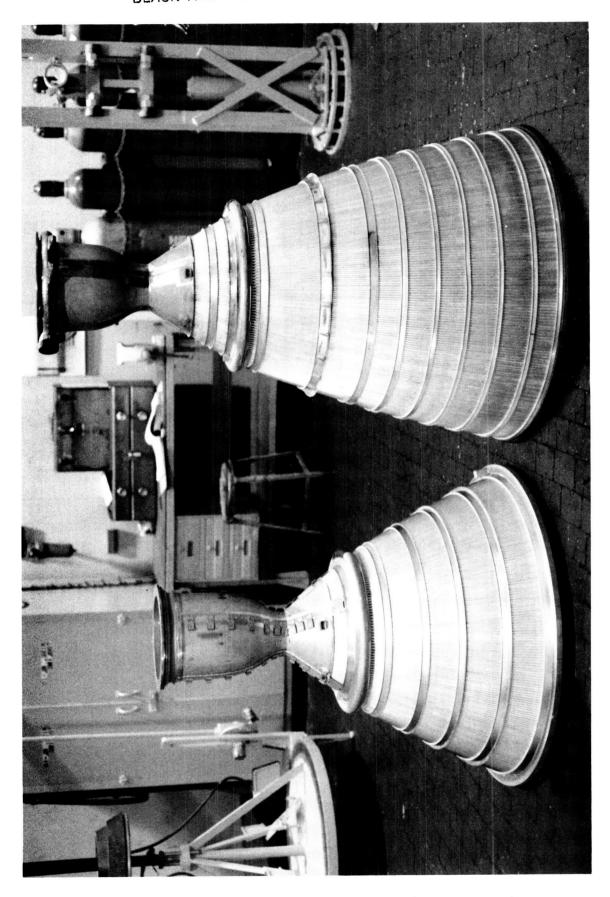


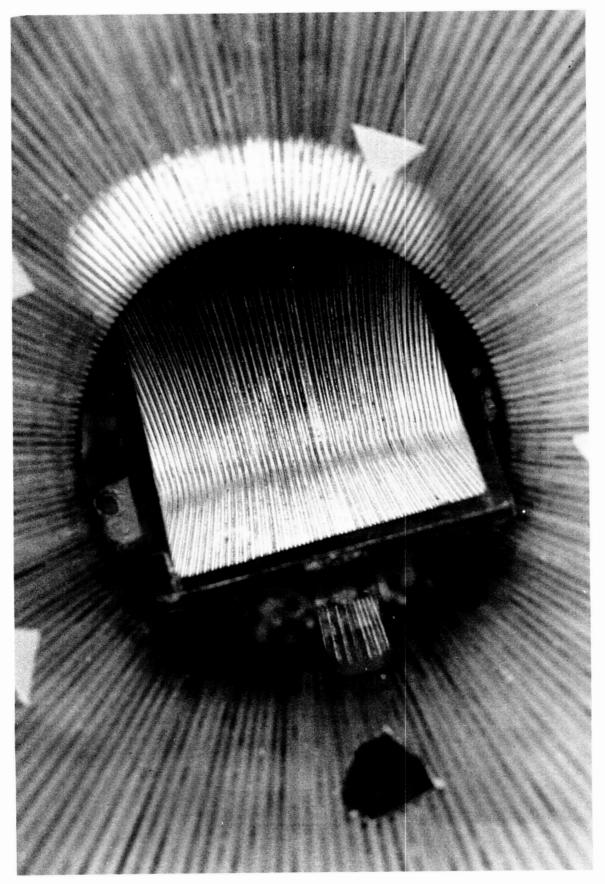
Figure 63. Post-Braze Exit Manifold Tube Sockets

Figure 64. Chamber/Primary Nozzle — RL10 Derivative II vs RL10A-3-3



ORIGINAL PAGE IS OF POOR QUALITY

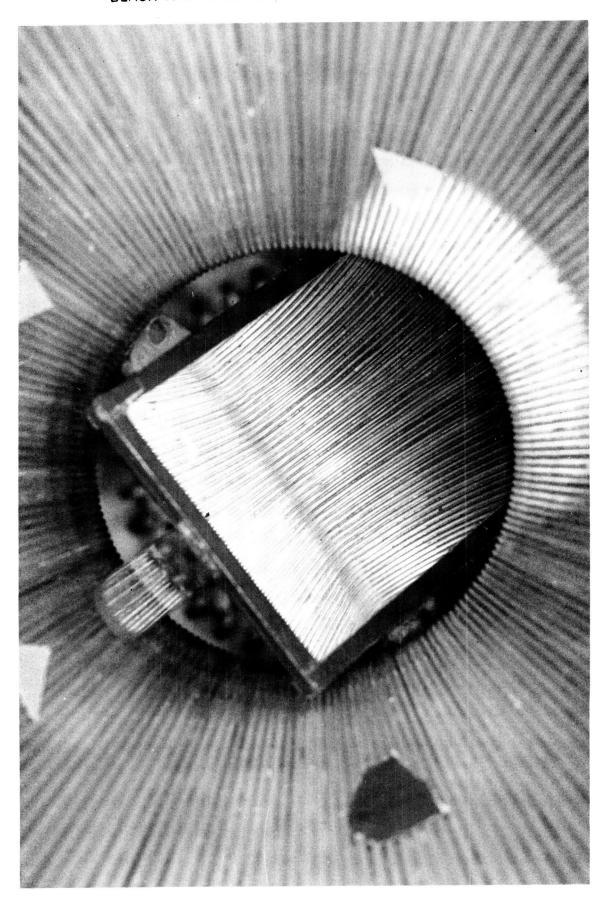
ATTACHMENT 3
THROAT AND INJECTOR FACE
PRIOR TO FIRST FIRING



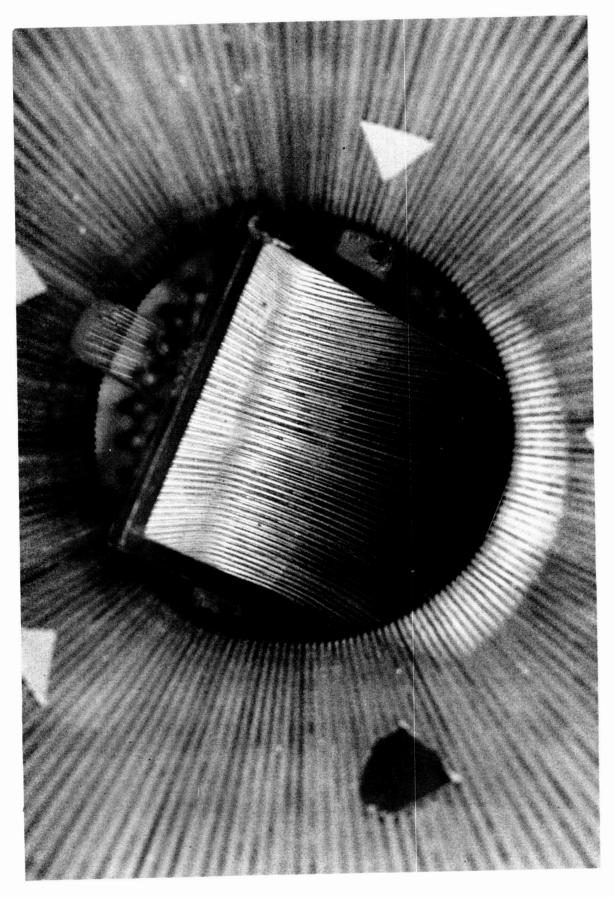
ORIGINAL PAGE BLACK AND WHITE PHOTOGRAPH

103

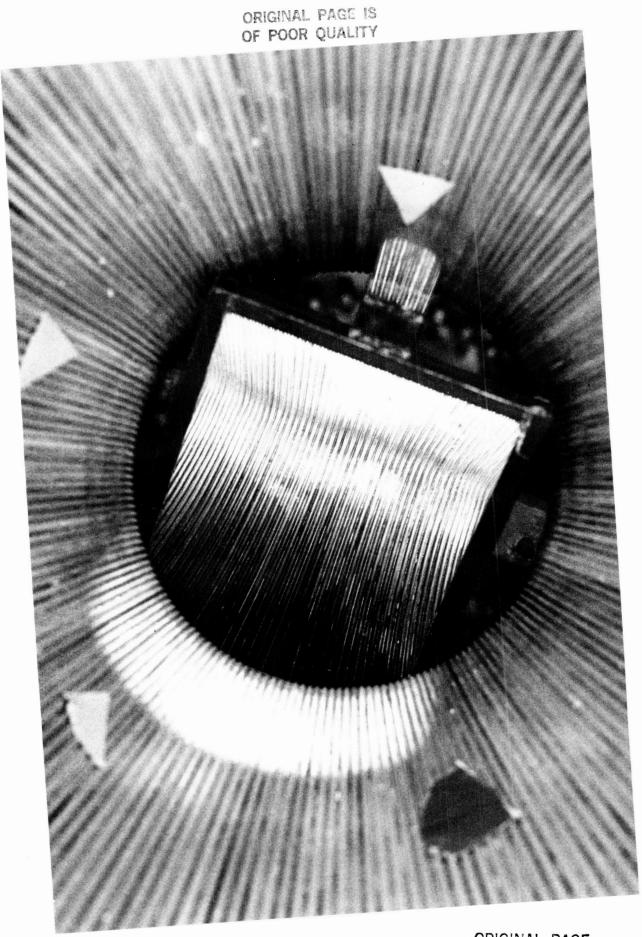
PAGE 102 INTENTIONALLY BLANK



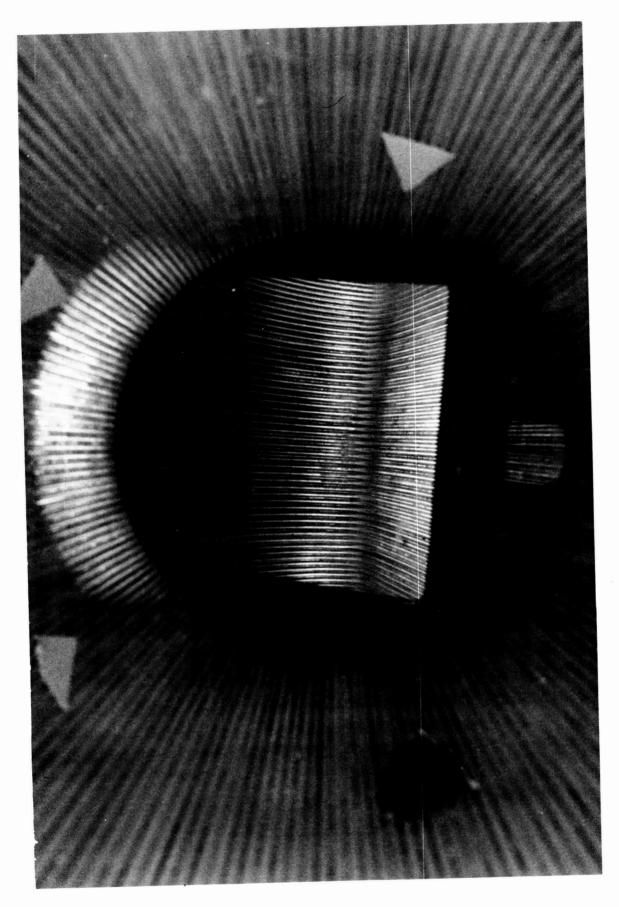
ORIGINAL PAGE IS OF POOR QUALITY



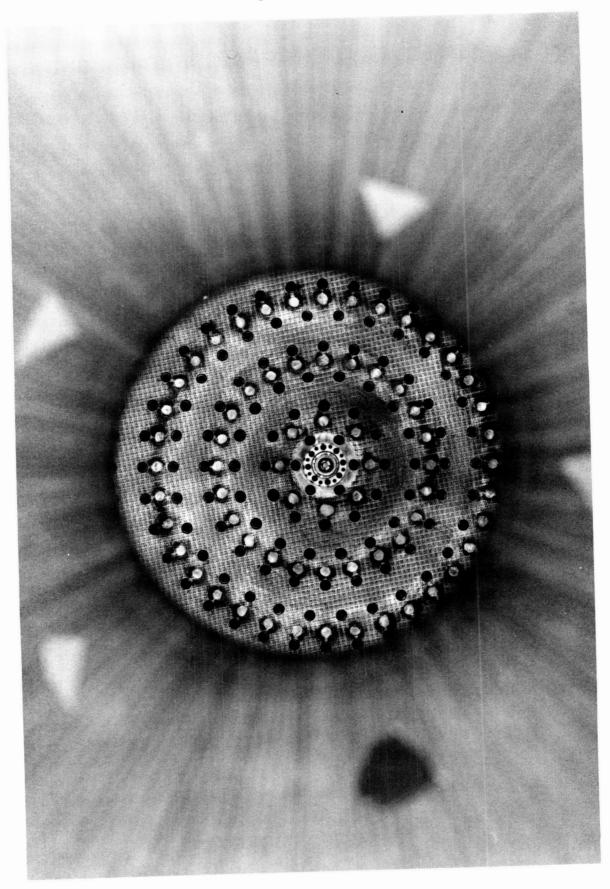
ORIGINAL PAGE
BLACK AND WHITE PHOTOGRAPH



ORIGINAL PAGE BLACK AND WHITE PHOTOGRAPH

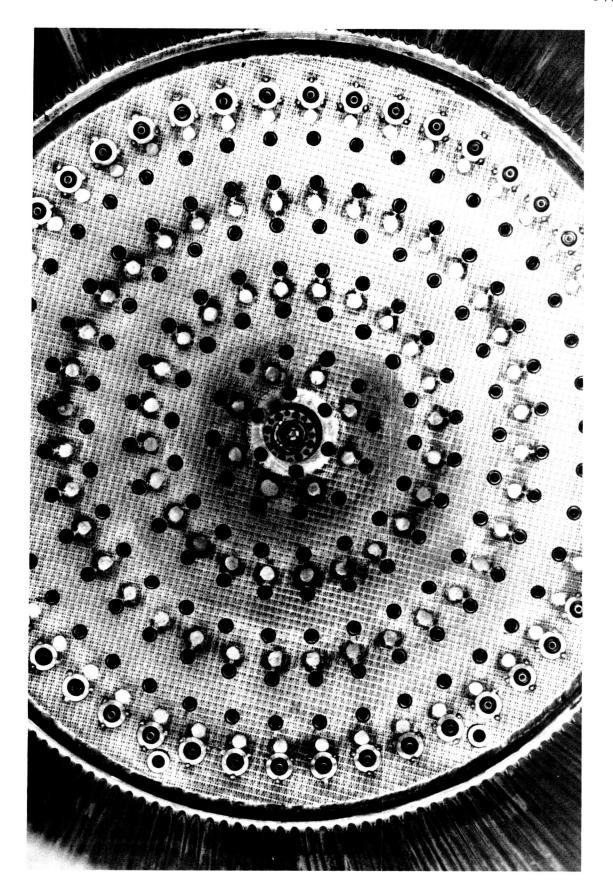


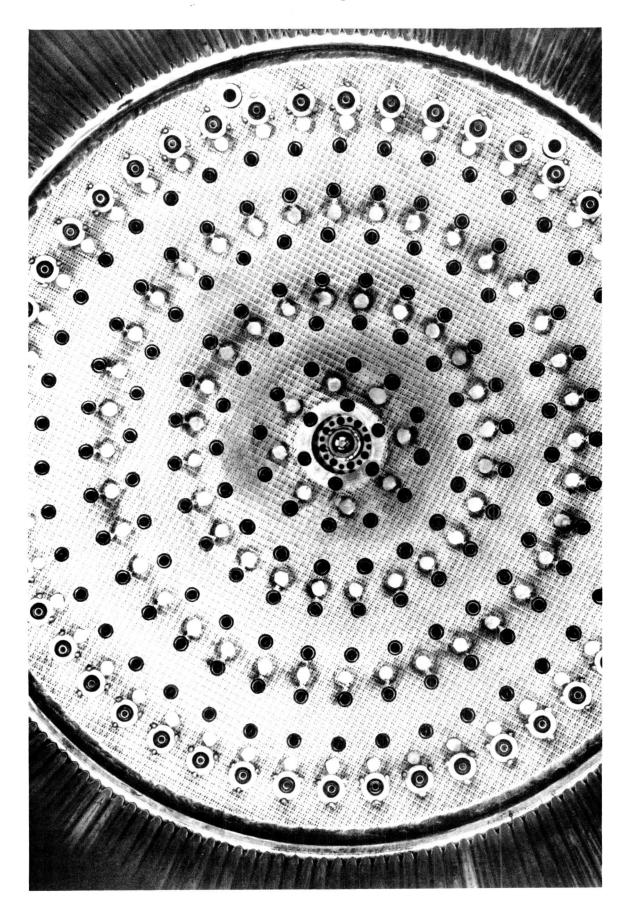
ORIGINAL PAGE BLACK AND WHITE PHOTOGRAPH



ORIGINAL PAGE
BLACK AND WHITE PHOTOGRAPH

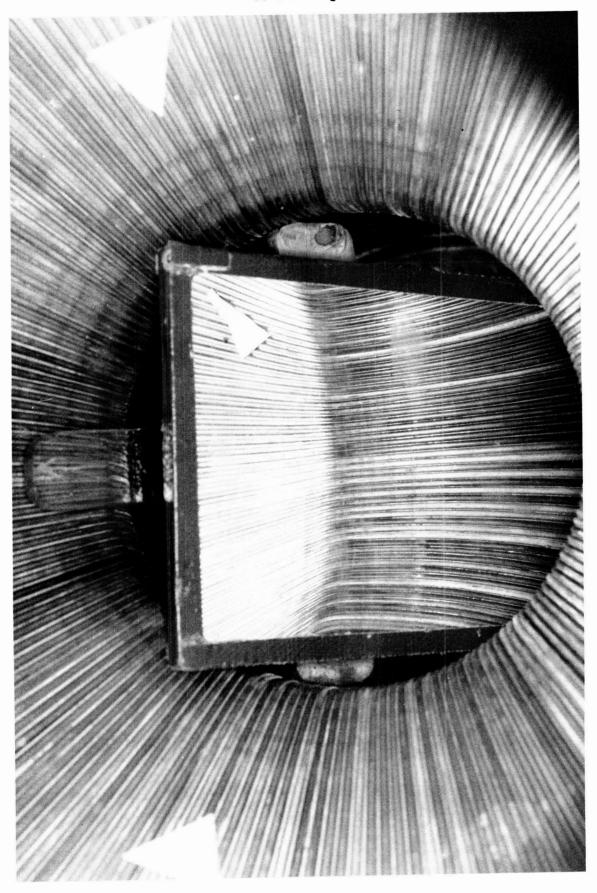
ATTACHMENT 4
INJECTOR FACE, THROAT AND PRIMARY NOZZLE INTERIOR
AFTER FIRST FIRING — HR 65.01



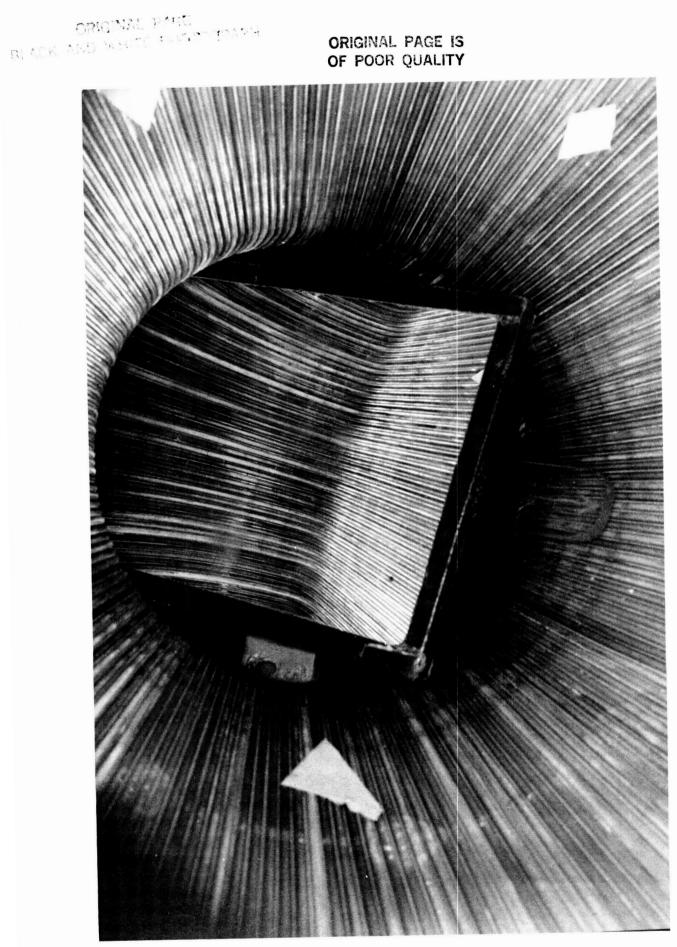




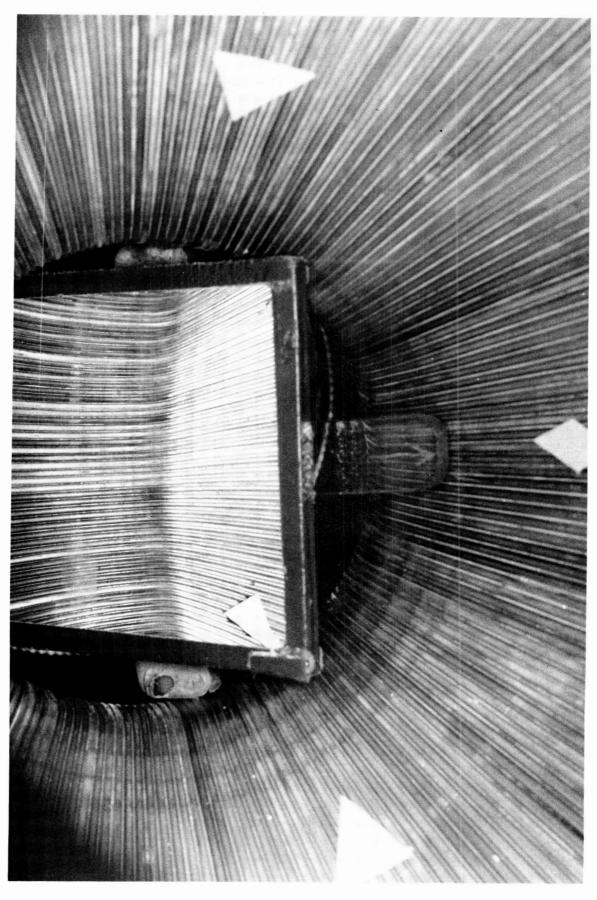
ORIGINAL PAGE
BLACK AND WHITE PHOTOGRAPH



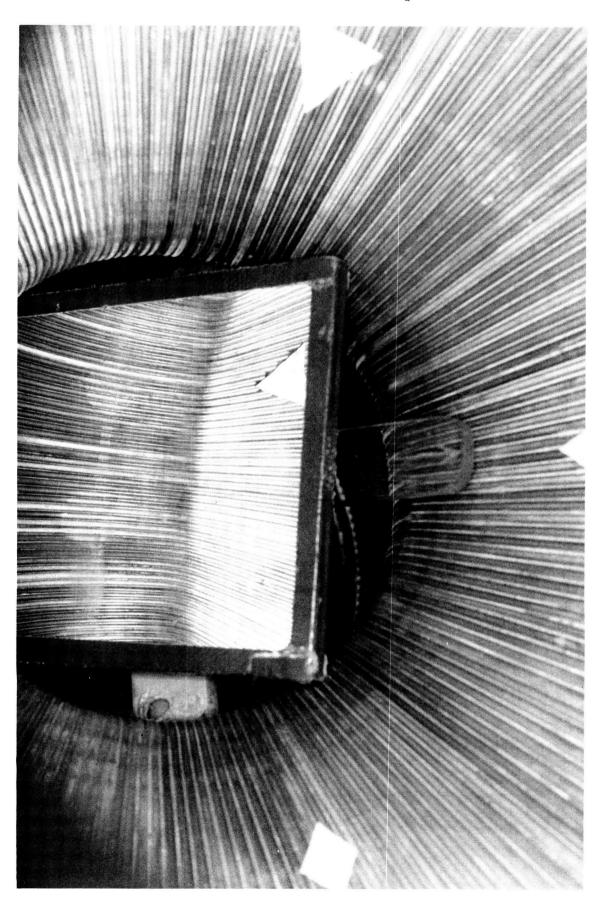
ORIGINAL PAGE
BLACK AND WHITE PHOTOGRAPH



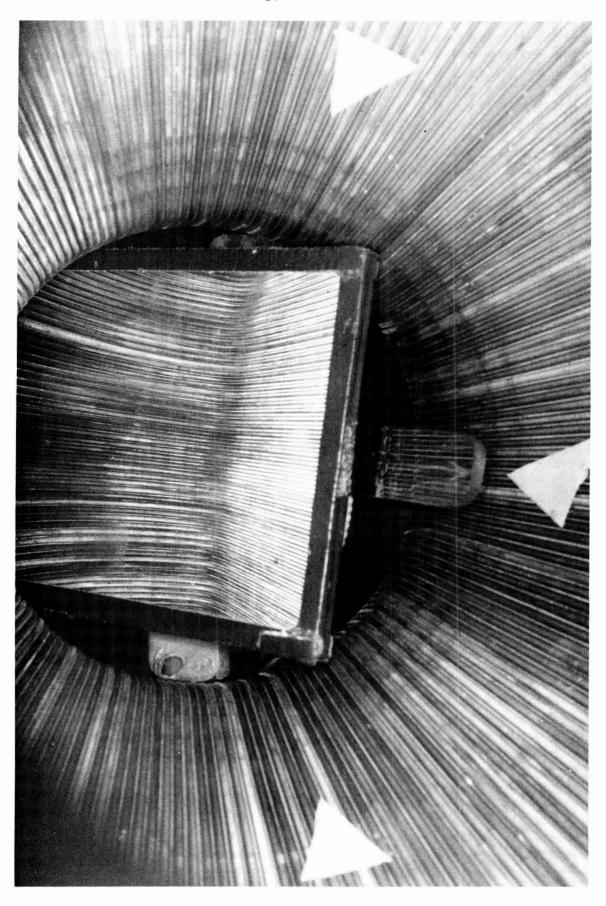
ORIGINAL PAGE BLACK AND WHITE PHOTOGRAPH



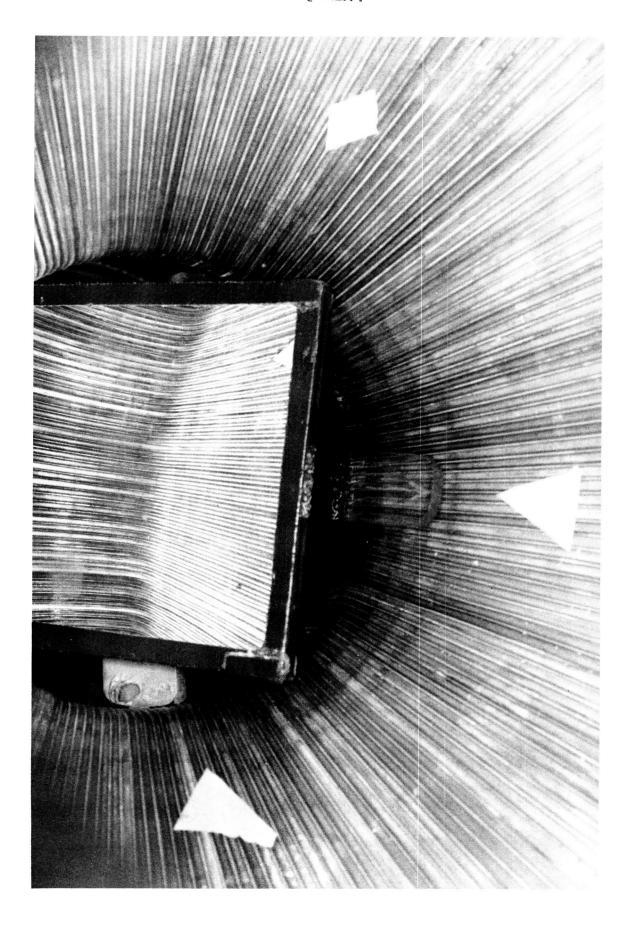
ORIGINAL PAGE
BLACK AND WHITE PHOTOGRAPH



ORIGINAL PAGE BLACK AND WHITE PHOTOGRAPH

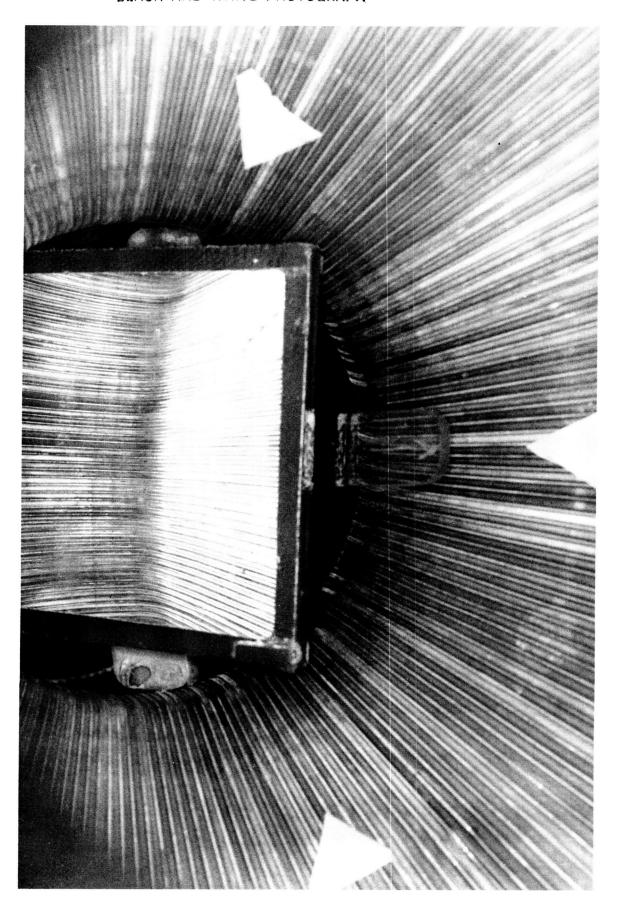


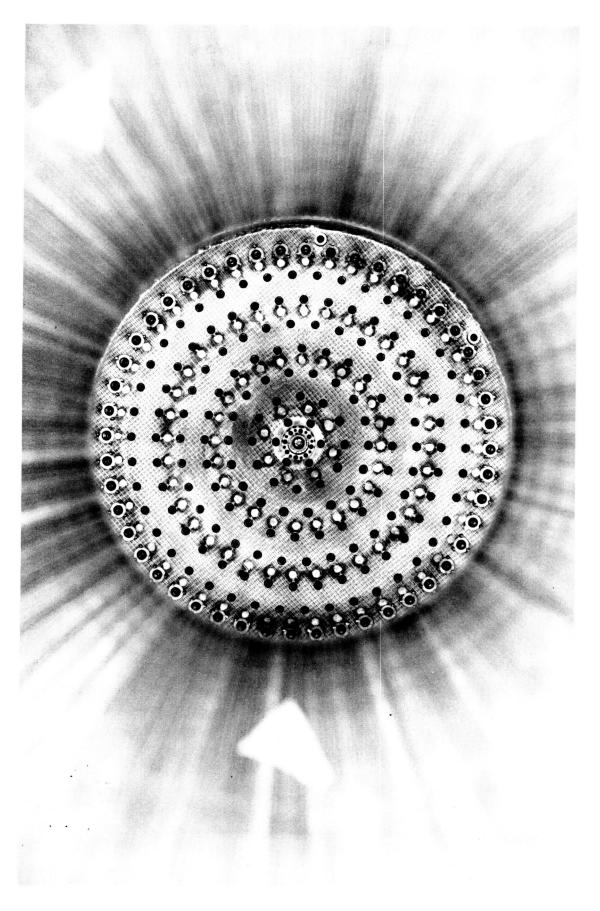
ORIGINAL PAGE BLACK AND WHITE PHOTOGRAPH



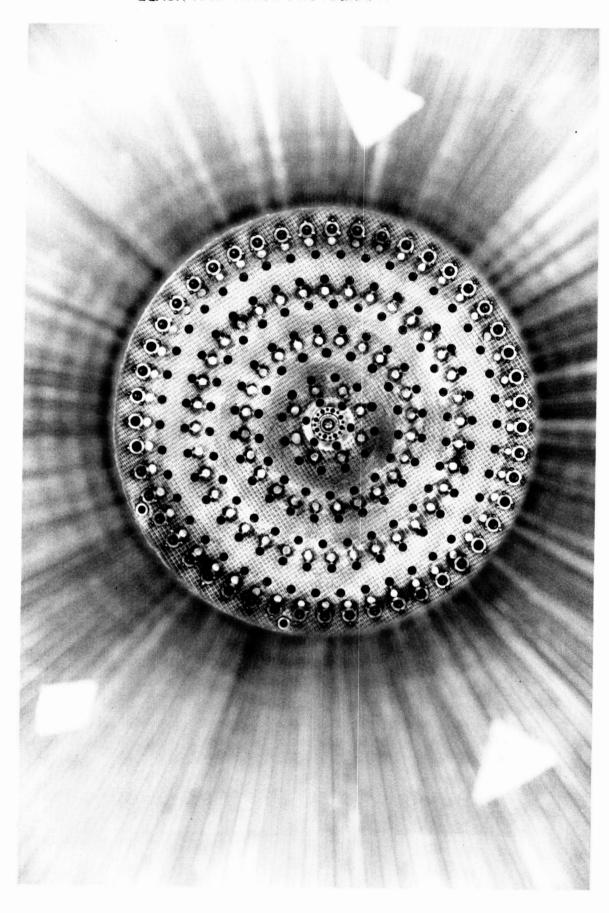
ORIGINAL PAGE Black and white Photograph

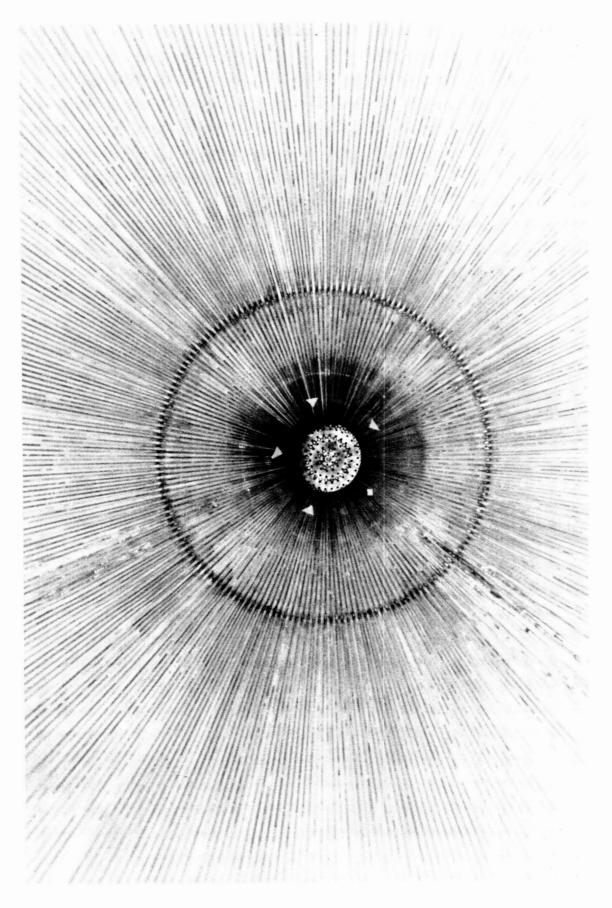
ORIGINAL PAGE BLACK AND WHITE PHOTOGRAPH





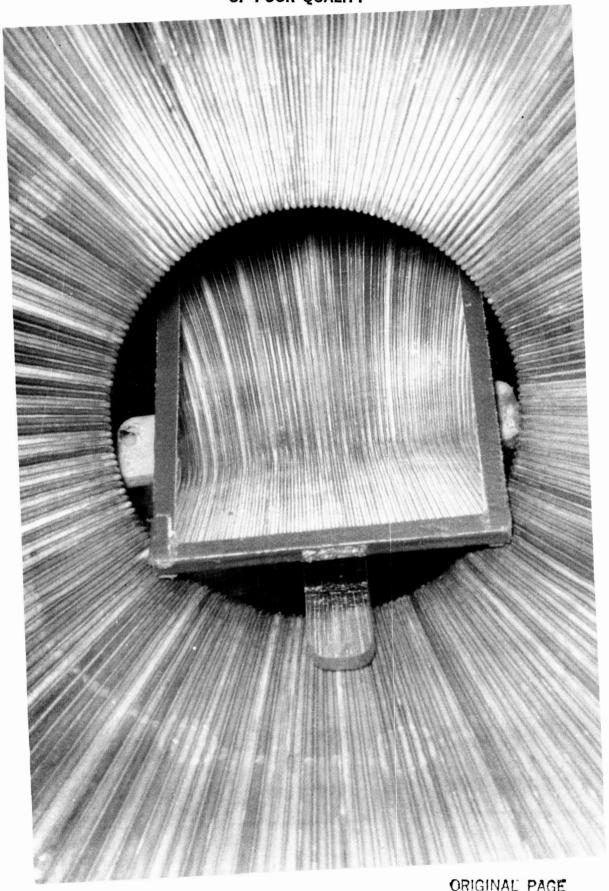
ORIGINAL PAGE BLACK AND WHITE PHOTOGRAPH





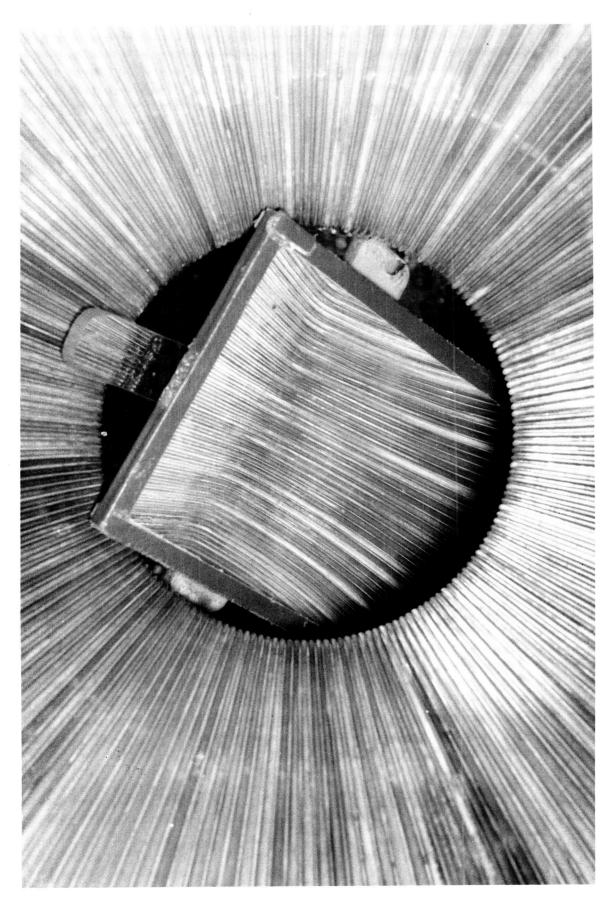
ATTACHMENT 5 INJECTOR FACE, COMBUSTION CHAMBER, AND THROAT AFTER FINAL TEST — HR 68.01

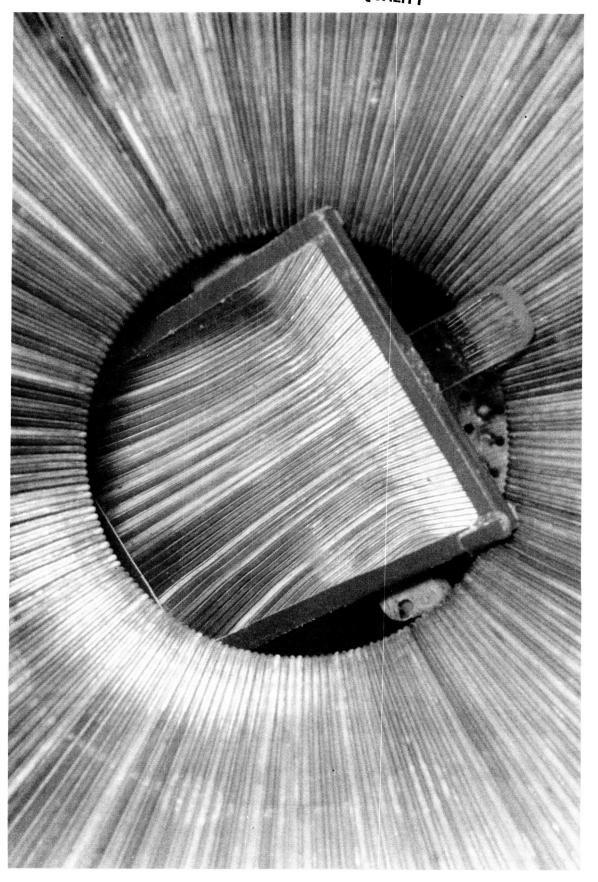
PRECEDING PAGE BLANK NOT FILMED



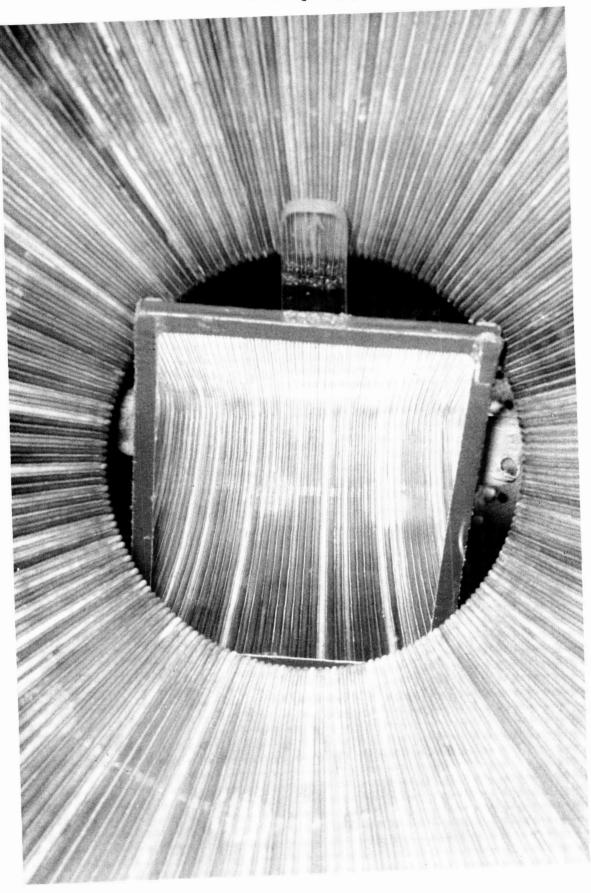
ORIGINAL PAGE BLACK AND WHITE PHOTOGRAPH

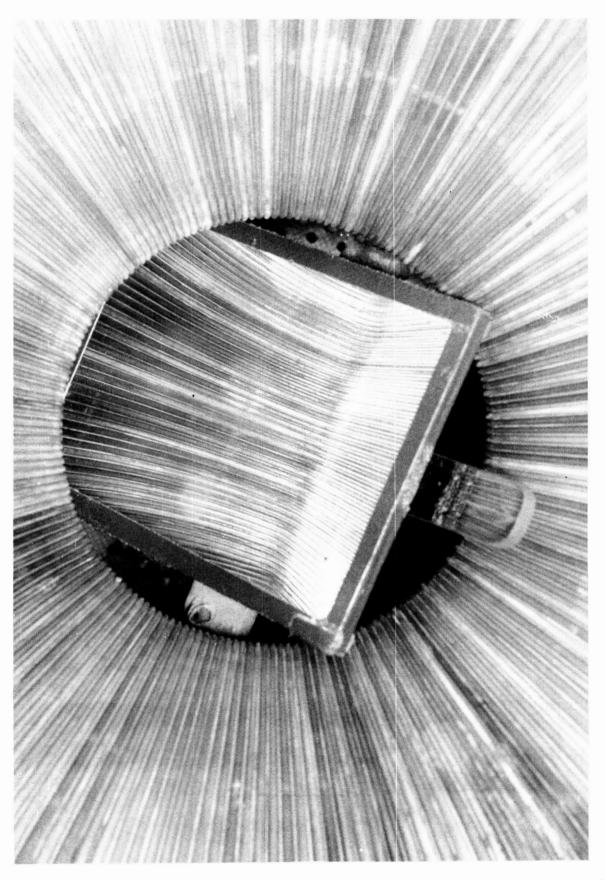
ORIGINAL PAGE BLACK AND WHITE PHOTOGRAPH



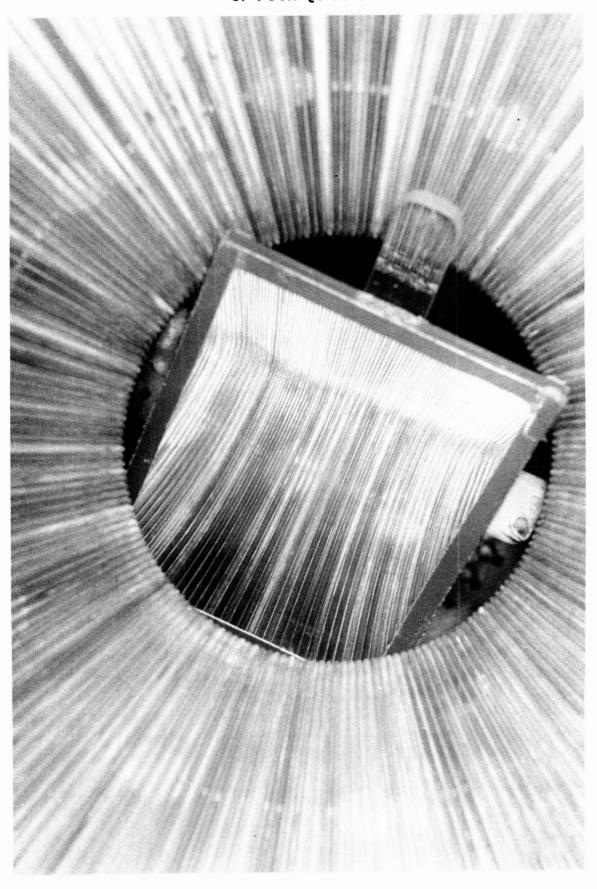


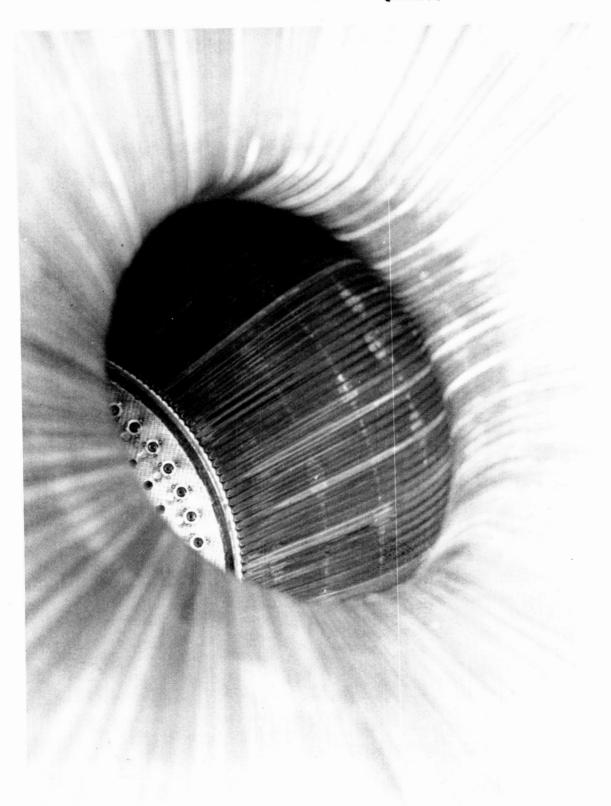
ORIGINAL PAGE BLACK AND WHITE PHOTOGRAPH

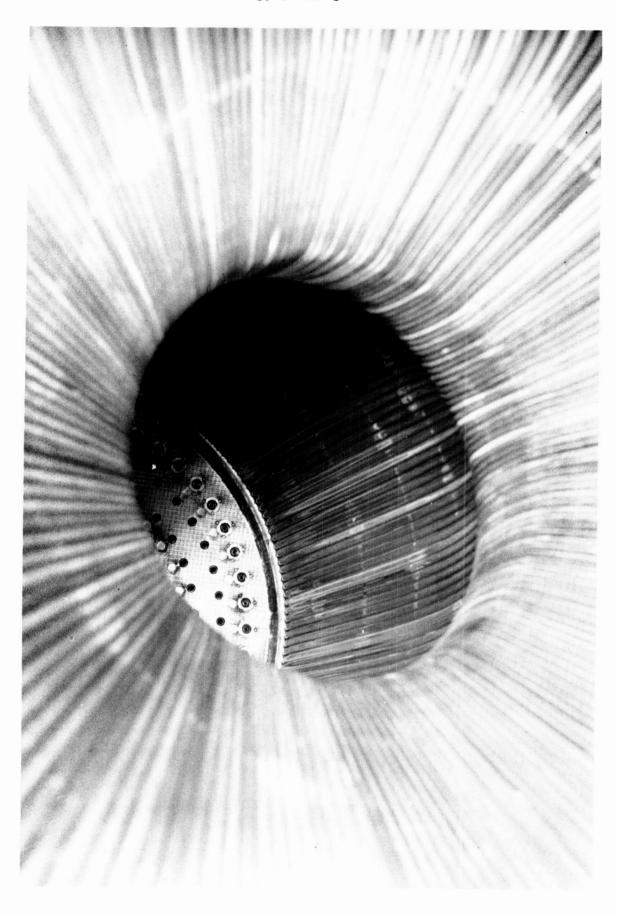




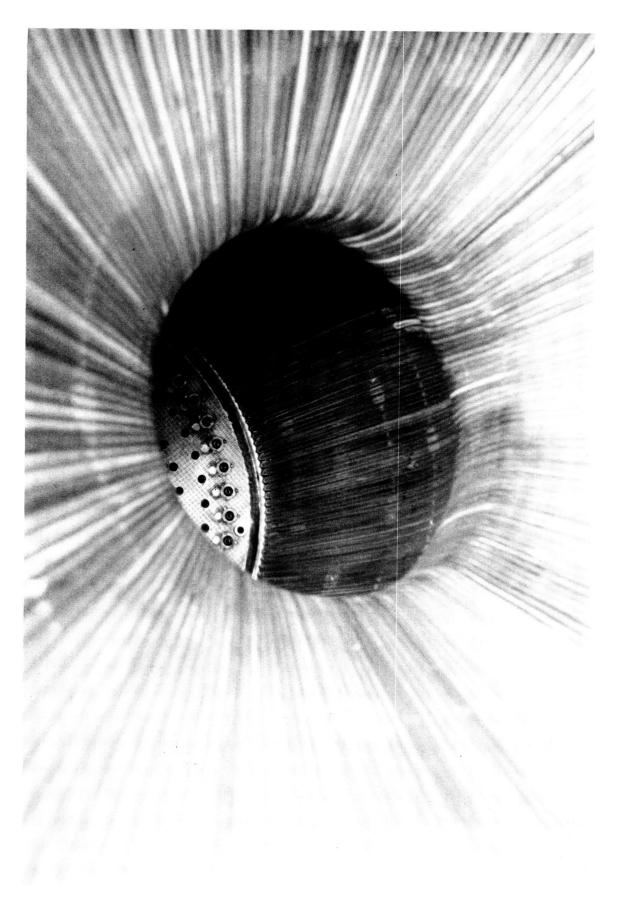
ORIGINAL PAGE BLACK AND WHITE PHOTOGRAPH

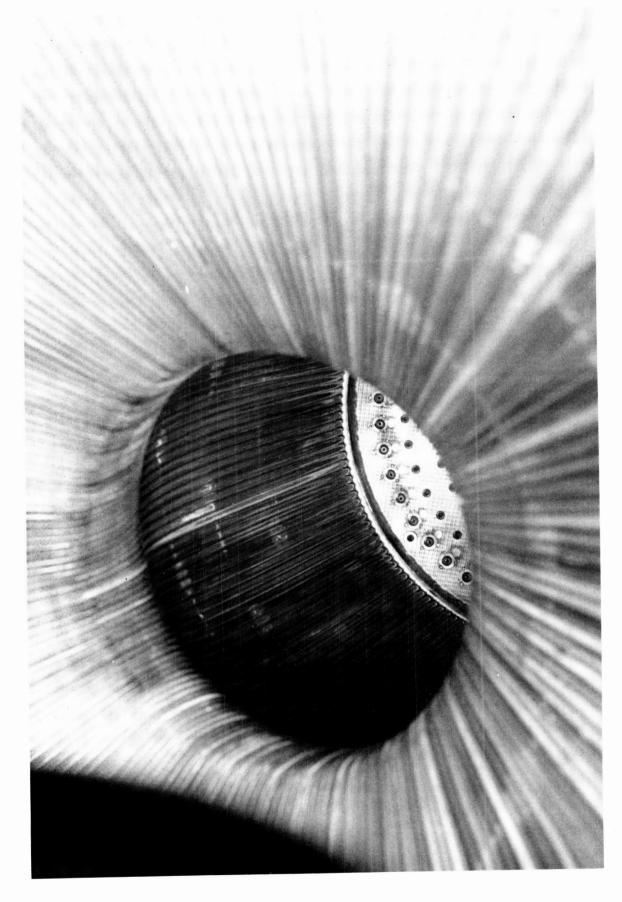




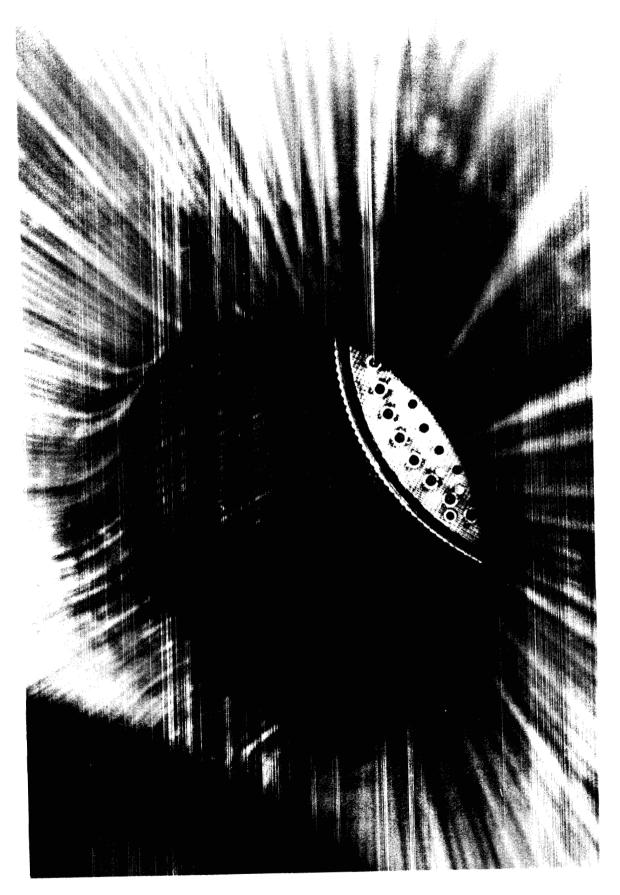


ORIGINAL PAGE BLACK AND WHITE PHOTOGRAPH

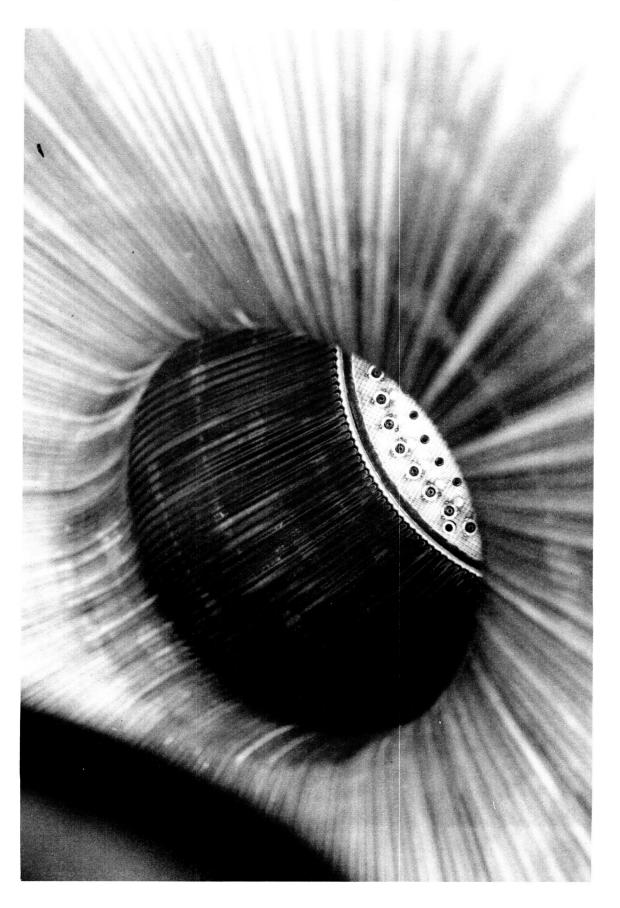




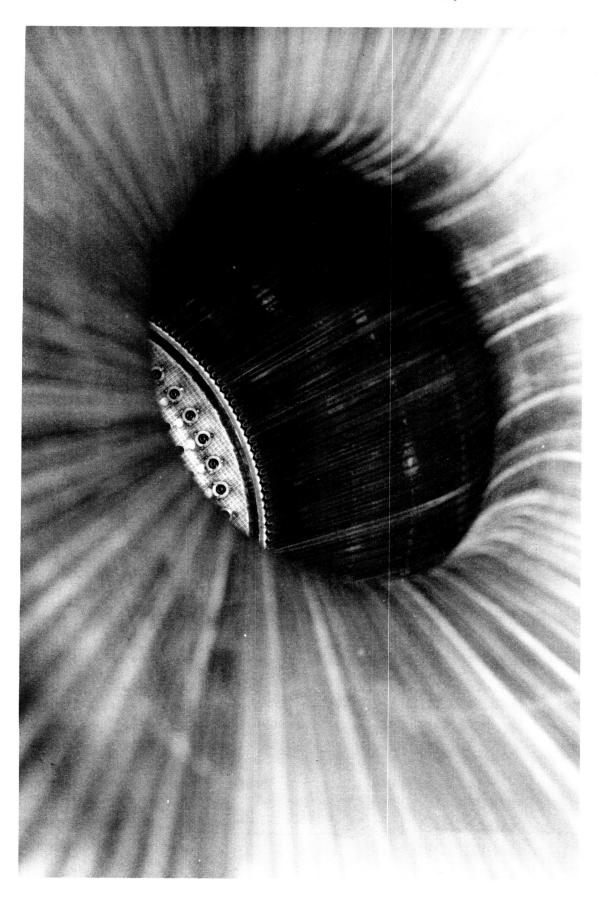
ORIGINAL PAGE BLACK AND WHITE PHOTOGRAPH



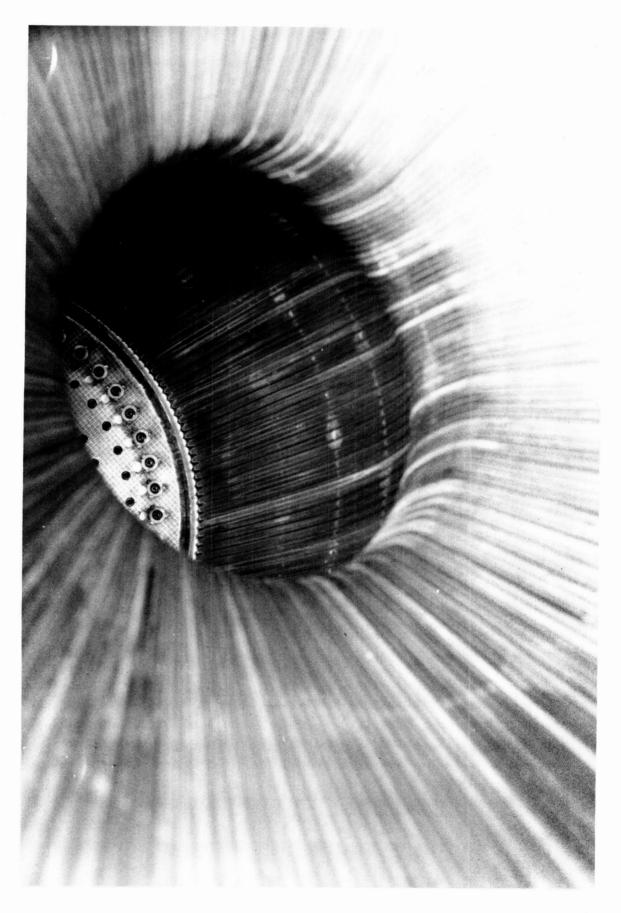
ORIGINAL PAGE
BLACK AND WHITE PHOTOGRAPH



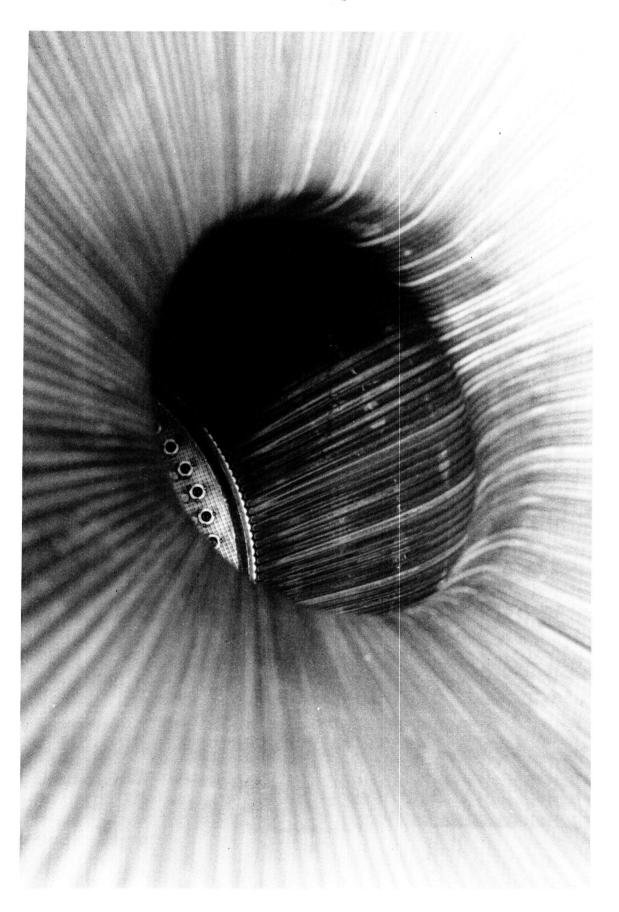
ORIGINAL PAGE BLACK AND WHITE PHOTOGRAPH



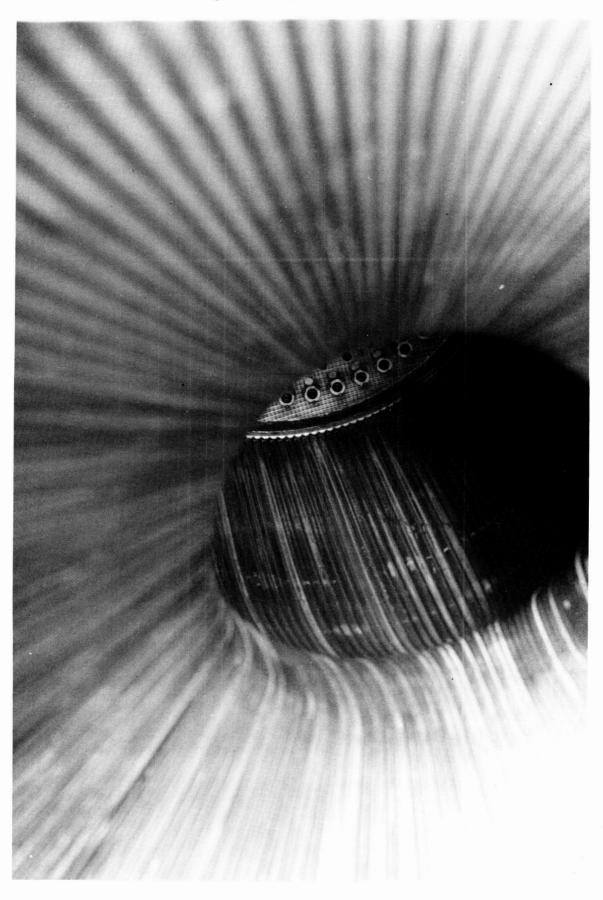
ORIGINAL PAGE BLACK AND WHITE PHOTOGRAPH



ORIGINAL PAGE
BLACK AND WHITE PHOTOGRAPH



ORIGINAL PAGE BLAGK AND WHITE PHOTOGRAPH



142

ORIGINAL PAGE BLACK AND WHITE PHOTOGRAPH

1. Report No.	2. Government Accession No.	3	. Recipient's Catalog No).
CR-170595				
4. Title and Subtitle		5	. Report Date	
The Design, Fabrication	and Test of the RL10 Ch	amber/	January, 1987	
Primary Nozzle			. Performing Organization	on Code
7. Author(s)		8	. Performing Organization	on Report No.
R. W. Marable			FR-19625	
		10	. Work Unit No.	
9. Performing Organization Name and Add	ress	11	. Contract or Grant No.	
Pratt and Whitney Aircra P.O. Box 109600	ft	'	NAS3-24738	
West Palm Beach, FL 334	10-9600	12	. Type of Report and Per	riad Cayerad
			Topical F.	
12. Sponsoring Agency Name and Address NASA-Lewis Research Cent	or		11/84 -	
21000 Brookpark Road	er	14	. Sponsoring Agency Co	de
Cleveland, OH 44135				
accomplished as part of		ement Progra	am (PIP). The	overall
accomplished as part of goal of the RL10 PIP was new cryogenic upper stag would be reached by prod	the RL10 Product Improve to gain the knowledge e engines to fulfill fu ucing an RL10 engine de	ement Progra and experien ture NASA re signed to be	am (PIP). The nce necessary equirements. e reusable, op	overall to develop The goal erate at
several thrust levels, a primary nozzle Task were increased mixture ratio new or updated technique the design and construct	(1) to design a reusabland low thrust, (2) to s where possible, and (le assembly fabricate th	capable of op aree assemblie	eration at s using
The design and far features such as single and relocated tube exit computer program was dev and heat transfer requir	braze joints (i.e., hoo) eloped to design the ch	segments (i ked tube ex:	.e., Mae West it). In addit	segments)
The test phase she be as predicted. These sufficiently proved the chamber/primary nozzle a	overall design of the R	heat transf	er data obtai	ned,
7. Key Words (Suggested by Author(s)) Space Propulsion Systems	Expander Cycle	tribution Statement		
Variable Thrust Rockets Liquid Propellant Rocket	Engines			
Hydrogen/Oxygen Engine		General	Release	
Hydrogen/Oxygen Technolog	ay			
9. Security Classif. (of this report)	20. Security Classif. (of this page)		21. No. of pages	22. Price*
Unclassified	Unclassified		142	